ARMY RESEARCH LABORATORY

Development of an Air Gun Simulation Model Using LS-DYNA

by Mostafiz R. Chowdhury and Ala Tabiei

ARL-TR-3016 July 2003

NOTICES

Disclaimers

The findings in this report are not to be construed as an official Department of the Army position unless so designated by other authorized documents.

Citation of manufacturer's or trade names does not constitute an official endorsement or approval of the use thereof.

Destroy this report when it is no longer needed. Do not return it to the originator.

Army Research Laboratory
Aberdeen Proving Ground, MD 21005-5069

ARL-TR-3016 **July 2003**

Development of an Air Gun Simulation Model Using LS-DYNA

Mostafiz R. Chowdhury
Weapons and Materials Research Directorate, ARL

Ala Tabiei
Consultant

Report Documentation Page

Form Approved
OMB No. 0704-0188

1. REPORT DATE *(DD-MM-YYYY)*	2. REPORT TYPE	3. DATES COVERED (From - To)
July 2003	Final	11 June 2002–30 September 2002

4. TITLE AND SUBTITLE
Development of an Air Gun Simulation Model Using LS-DYNA

5a. CONTRACT NUMBER

5b. GRANT NUMBER

5c. PROGRAM ELEMENT NUMBER

6. AUTHOR(S)
Mostafiz R. Chowdhury and Ala Tabiei*

5d. PROJECT NUMBER
DCST000

5e. TASK NUMBER

5f. WORK UNIT NUMBER

7. PERFORMING ORGANIZATION NAME(S) AND ADDRESS(ES)
U.S. Army Research Laboratory
ATTN: AMSRL-WM-MB
Aberdeen Proving Ground, MD 21005-5069

8. PERFORMING ORGANIZATION REPORT NUMBER
ARL-TR-3016

9. SPONSORING/MONITORING AGENCY NAME(S) AND ADDRESS(ES)

10. SPONSOR/MONITOR'S ACRONYM(S)

11. SPONSOR/MONITOR'S REPORT NUMBER(S)

12. DISTRIBUTION/AVAILABILITY STATEMENT
Approved for public release; distribution is unlimited.

13. SUPPLEMENTARY NOTES
* 4056 Granite Ct., Mason, OH 45040

14. ABSTRACT

This report presents an analytical methodology to simulate the dynamic impact response of a generic artillery component subjected to launch simulation in an air gun test environment. An air gun test provides an efficient and effective launch simulation platform designed for testing suitability and survivability of future artilleries or projectile components during their developmental stage. Lagrangian and Aribitrary Lagrangian/Eulerian methods are used to simulate the impact mitigation environment in which the kinetic energy of a projectile is absorbed by crushing aluminum (Al) honeycomb mitigator. Issues related to the effectiveness of these methods in simulating a high degree of distortion of Al honeycomb mitigator using the available LS-DYNA material models 126 (metallic honeycomb) and 63 (crushable foam) are discussed. Both computational methods lead to the same prediction for the deceleration of the test projectile and are able to simulate the behavior of the projectile. Good agreement between the test results and the predicted projectile response is achieved using the presented models and the methods employed. Development of such a simulation code significantly enhances the U.S. Army Research Laboratory's capability in addressing the customer's need in explaining projectile behavior during an air gun test and is useful in facilitating design and preparation of an effective air gun test.

15. SUBJECT TERMS
air gun simulation, Al honeycomb mitigator, Lagrangian/Arbitrary Lagrangian-Eulerian FE method, correlation, LS-DYNA, gun launch simulation

16. SECURITY CLASSIFICATION OF:			17. LIMITATION OF ABSTRACT	18. NUMBER OF PAGES	19a. NAME OF RESPONSIBLE PERSON
a. REPORT	b. ABSTRACT	c. THIS PAGE			Mostafiz R. Chowdhury
UNCLASSIFIED	UNCLASSIFIED	UNCLASSIFIED	UL	52	19b. TELEPHONE NUMBER *(Include area code)* 301-394-6308

Contents

List of Figures

List of Tables

Acknowledgments

The analytical work presented here was accomplished under a contract (Contract no. DAAD19-02-D-0001, TCN 02-125) with the Scientific Services Program (STAS), U.S. Army Research Office, Research Triangle Park, NC. Air gun tests were conducted by Ara Abrahamian, U.S. Army Research Laboratory (ARL), Weapons and Materials Research Directorate (WMRD), Adelphi, MD. Contributions of Ara Abrahamian, Edward Szymanski, and William McIntosh of WMRD, ARL in delivering the air gun test are greatly appreciated.

Summary

This report presents an analytical methodology to simulate the dynamic impact response of a generic artillery component subjected to launch simulation in an air gun test environment. An air gun test provides an efficient and effective launch simulation platform designed for testing suitability and survivability of future artilleries or projectile components during their developmental stage. LS-DYNA models are developed to simulate the impact mitigation environment in which the kinetic energy of a projectile is absorbed by crushing aluminum (Al) honeycomb mitigator. Two computational methods are used for the simulation: Lagrangian and Aribitrary Lagrangian/Eulerian (ALE). This report discusses the advantages, disadvantages, and the effectiveness of these methods in simulating a high degree of distortion of Al honeycomb mitigator. Both computational methods lead to the same prediction for the deceleration of the test projectile. The Lagrangian method is simpler to set up, postprocess, and requires less computational time than the ALE method. However, it requires significant expertise to make the simulation numerically stable. On the other hand, the ALE method is more difficult to set up, postprocess, and requires much more CPU time. An ALE simulation is more suitable for very large deformation problems such as those involving material flow.

The Al honeycomb mitigator is modeled using two material models available in LS-DYNA simulation code. Both material models 126 (metallic honeycomb) and 63 (crushable foam) lead to reasonable predictions and are able to simulate the behavior of the projectile. The strain rate sensitivity is found to be an important factor in these simulations. Good agreement between the test results and the predicted projectile response is achieved using the presented models and the methods employed. Development of such a simulation code significantly enhances the U.S. Army Research Laboratory's (ARL's) capability to address the customer's need in explaining projectile behavior during an air gun test and is useful in facilitating design and preparation of an effective air gun test.

INTENTIONALLY LEFT BLANK.

1. Introduction

ARL's air gun facility has been used widely for testing suitability and survivability of future artilleries or projectile components during their developmental phase. An air gun test provides an efficient and effective launch simulation platform in which the shock phenomena in a real gun test are replicated in a controlled environment. The primary focus of such an air gun mitigation test is to simulate a transient shock environment that the test item is anticipated to sustain in an actual field test. Proper simulation of the gun launch environment using an air gun test, thus, demands that the dynamics of the physical energy-absorbing interfacing components that regulate the shock environment are properly understood. Currently, a rigid-body simulation-based predictor-corrector approach is used for selecting physical operating parameters in an air gun test. Physical design parameters are selected such that a target deceleration profile is attained during the gun launch simulation test. A rigid-body simulation-based approximate selection procedure fails to capture the dynamics of the projectile because of its innate simplifications. Development of a virtual simulation model capable of including gun launch dynamics is, thus, deemed essential in advancing ARL's air gun test capabilities and in meeting the customer's ever-increasing demand. This methodology requires developing a predictive model of responses of the test article. This report presents the development of a finite-element (FE) model to simulate the dynamic impact response of a generic artillery component mounted on a given projectile during gun launch simulation in an air gun test.

Several LS-DYNA models of a generic test article fired in a 4-in air gun chamber are developed in this study. Control test data for a test item mounted on a projectile are used for model validation and correlation. Analytical simulation of the air gun launch environment requires the modeling of an event in which the test object mounted on a projectile is launched and decelerated by crushing the Al honeycomb mitigator in the recovery chamber. As a secondary energy absorbing device, a momentum exchange mass (MEM) is used at the retrieving end. Two formulations are used in the simulations: Lagrangian and ALE. The Al honeycomb mitigator undergoes significant deformation that could render a severely unstable Lagrangian simulation. For this reason, an ALE simulation is also considered. The Eulerian method is more suitable for problems involved in severe mesh distortion. The Lagrangian method, on the other hand, is limited in how much an element can deform. The Lagrangian method is easy to set up and visualize since the material point moves with the mesh. The Eulerian method, however, is more difficult to set up, and the mesh is stationary so that material points are advected (flowed) from one element to the next.

The Al honeycomb mitigator is modeled with *MAT_MDIFIED_HONEYCOMB in the LS-DYNA simulation code. This is material model 126 in the code. This material model is available for the Lagrangian method only and it is not yet implemented in the Eulerian solver

of the LS-DYNA. Therefore, an alternative material model is considered that can simulate the behavior of Al honeycomb and is available in the LS-DYNA Eulerian solver. The material model considered for this case is *MAT_CRUSHABLE_FOAM, which is material model 63 in LS-DYNA. This material model can simulate an isotropic crushable material, while the *MAT_MDIFIED_HONEYCOMB can simulate orthotropic crushable material. Most of the Al honeycomb material in the air gun simulation is crushed axially. Therefore, the *MAT_CRUSHABLE_FOAM model is considered to be appropriate for this model. The two material models are described in detail in section 4.

2. Objective

The objective of this effort is to develop an updated and correlated analytical model to predict three-dimensional (3-D) transient response of a generic artillery component subjected to launch simulation in the ARL 4-in air gun facility. The simulation is achieved using impact mitigation techniques, whereby the component is propelled to a target inside a 4-in carrier equipped to measure component response during the simulation. The overall model includes all elements of the simulation apparatus that contribute to the total response of the test item carried by the air gun projectile during its course through its flight.

3. Air Gun Test Description

A schematic diagram for a typical air gun test setup is shown in Figure 1. The test setup consists of a stationary gun barrel, a projectile, and a dual energy-absorbing mechanism consisting of a mitigator and a MEM positioned at the recovery end. In a typical air gun mitigation test, the projectile—carrying the artillery components to be tested—is launched to impact an Al honeycomb mitigator at the recovery chamber. On impacting the mitigator, the kinetic energy of the projectile is lessened by crushing the Al honeycomb mitigator. Crushed mitigator in turn exchanges its momentum to a MEM, a secondary energy-absorbing device, abutting its rear end.

A preshot arrangement of the dual energy absorbing devices in a 4-in air gun retrieving chamber is shown in Figure 2. As seen in the figure, the mitigator is stationed inside the split catch tube at the start of the test. The steel catch tube for the 4-in gun is 21 in long having an inner diameter (ID) of 4.025 in and an outer diameter (OD) of 6.062 in. Four 12.7-mm (0.5-in) diameter, 4340 steel tie rods (two on each side of the aisle, Figure 2) are used to fasten the top-half of the split catch tube with the stationary bottom-half shown in the figure. Bolts are 88.9 mm (3.5 in) from the ends of the catch tube. The striking end of the 0.6087 g/cm^3 (38 pcf) Al honeycomb

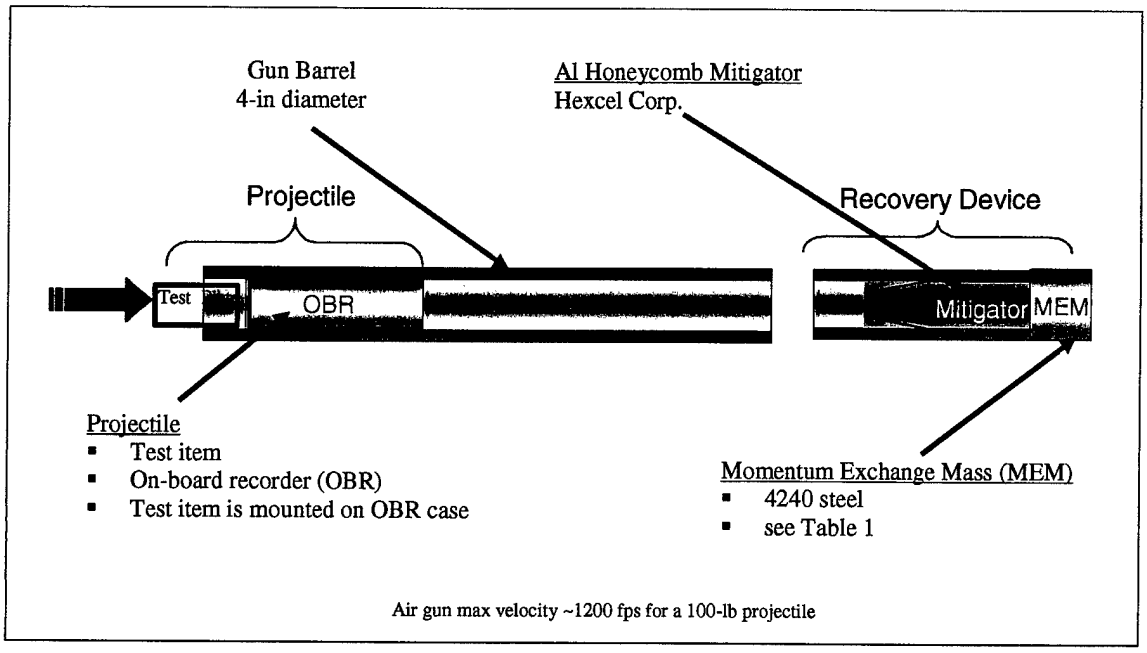

Figure 1. Schematic of a typical air gun test setup.

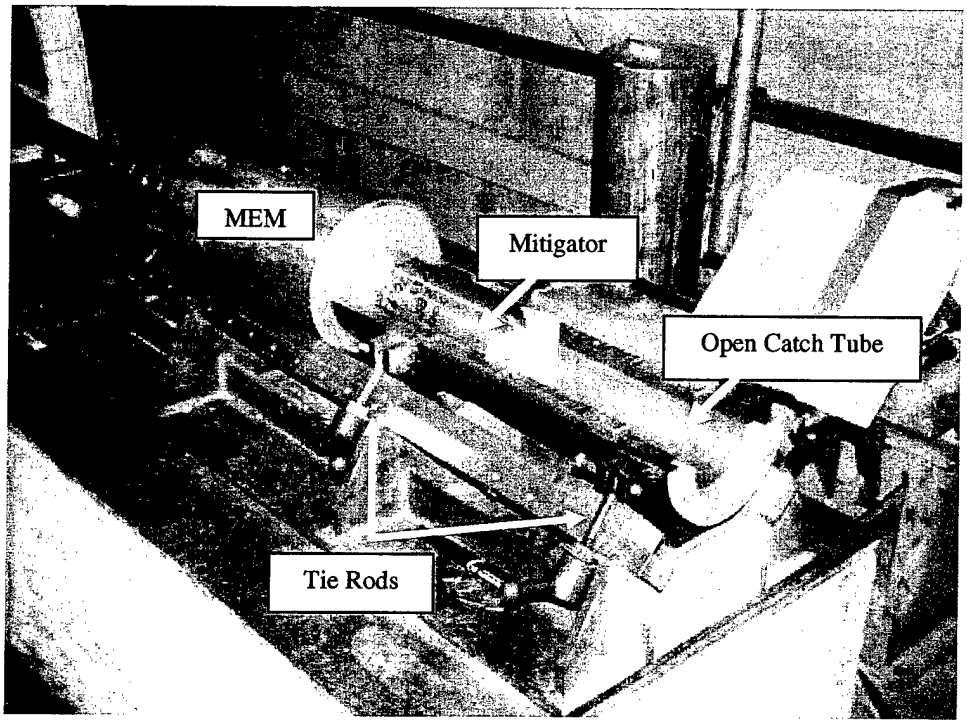

Figure 2. A preshot arrangement in the 4-in air gun test.

mitigator was fashioned to form two sharp wedges. With two such wedges at the striking end, the mitigator tends to crush evenly across its face. The length of the wedges also determines the projectile's deceleration profile during the impact. On initiation of an air gun shot, the test

projectile is launched from the breech chamber and is retrieved in the recovery chamber. A postshot relative position for the physical apparatus is shown in Figure 3. As seen in this figure, on hitting its target, the projectile remains trapped in the catch tube, the mitigator crushes, and the MEM displaces. An enlarged view of the crushed mitigator and the undeformed test projectile is shown in Figure 4.

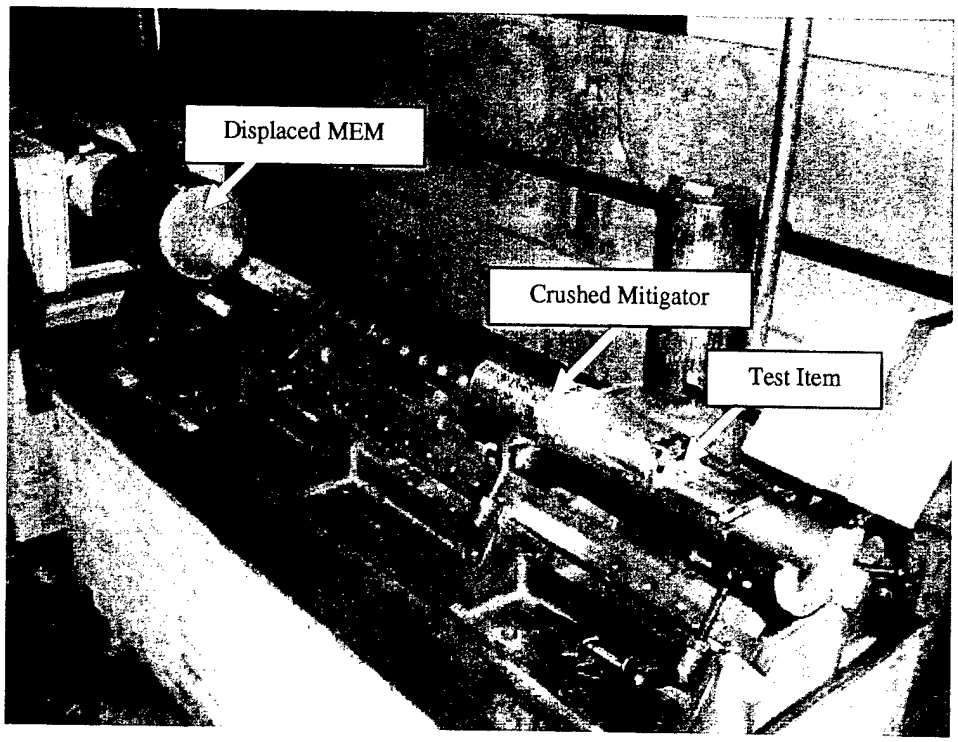

Figure 3. A postshot configuration of interacting components in a 4-in air gun test.

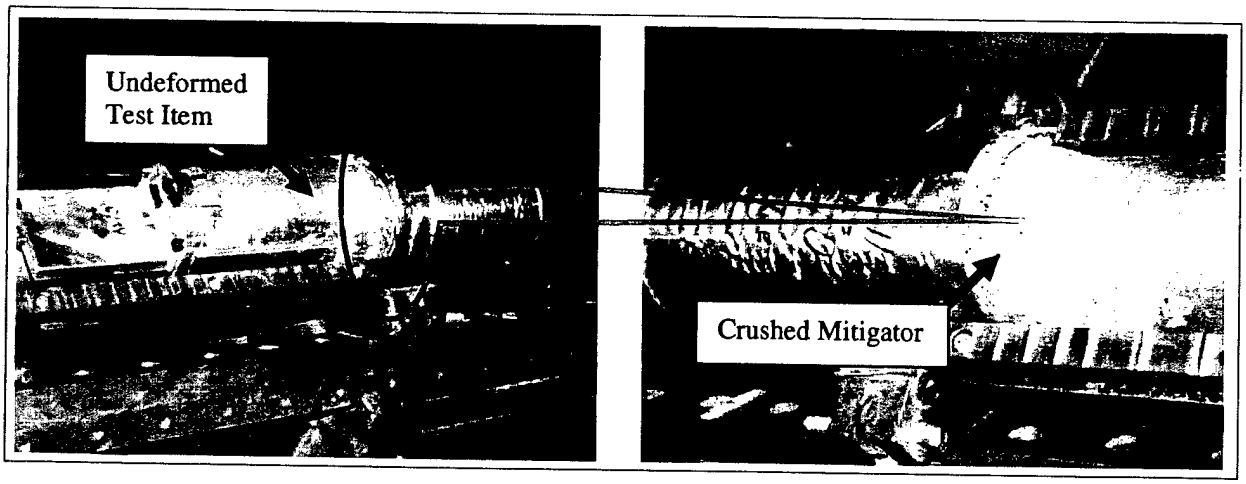

Figure 4. A postshot view of an Al crushed mitigator.

A test projectile—consisting of a rectangular Al plate mounted on the top of an on-board recorder (OBR) case—was specially prepared for FE verification. The projectile included the OBR carrier and a rectangular plate mounted on its top. In this test projectile, the OBR records the data and the plate is the test item, representing a simulated projectile component that could be used in an actual air gun test. The following are basic dimensions for the test projectile:

- Outer diameter = 101.09 mm (3.98 in),
- Inner diameter = 75.95 mm (2.99 in),
- Length = 152.4 mm (6 in),
- Wall thickness = 12.7 mm (0.5 in),
- End cap thickness = 25.4 mm (1 in),
- Top cap thickness = 12.7 mm (0.5 in), and
- Test plate dimension: 101.0 mm (4 in) × 76.2 mm (3 in) × 12.7 mm (0.5 in) Al plate, mounted on top cap.

Figure 5 shows the test projectile and the instrument locations for which the data were recorded using an on-board 12-bit, 4-channel high shock analog recorder placed inside the OBR case. Two accelerometers and two strain gages were mounted on the test item. The analog recorder was shock isolated inside the canister by suspending the device over glass beads and densely packed once the top mount had been assembled. Figure 6 shows the OBR assembly process for the test projectile. Packing the recorder with glass beads was an effective filtering mechanism in arresting propagation of the high-frequency shock wave from the container to the analog recorder. An isolated packaging arrangement was needed to ensure that the sensor data recorded during the flight were not contaminated by the recording device's own dynamics and also to ensure survival of the OBR.

Test data for three air gun shots were recorded in this study for subsequent FE model validation and verification purposes. Basic physical data for the recorded test shots are presented in Table 1. As indicated in the table, relative changes in the properties of the mitigator can substantially change the dynamic event of the air gun test. Shot 3, for example, was severe in its action and broke one of the tie rods that connected two halves of the catch tube, and the mitigator crushed the most. Filtered acceleration history for the top accelerometer for each shot is compared in Figure 7. Maximum peak acceleration for these shots ranged from 17,000 to 18,000 g's, where g is the acceleration due to gravity, 9.81 m/s^2 (32.2 ft/s^2).

Figure 5. An instrumented test projectile.

4. Material Models

The two material models considered here are materials 126 and 63 in LS-DYNA. The formulations of the two material models are described in detail in the following subsections. The input required for the two material models are described as well.

One of the most difficult aspects of this investigation was to define the material properties that would represent the physical behavior of the Al honeycomb mitigator used in the air gun test. In this investigation, no test was conducted for characterizing mitigator properties. Therefore, it was required to depend on the data available in the open literature. An experimental characterization of Al honeycomb material reported by Lu and Hinnerichs (*1*) was similar to the one that was used in this investigation. The crush test results available (*1*) were used to construct the material model used in the air gun simulations.

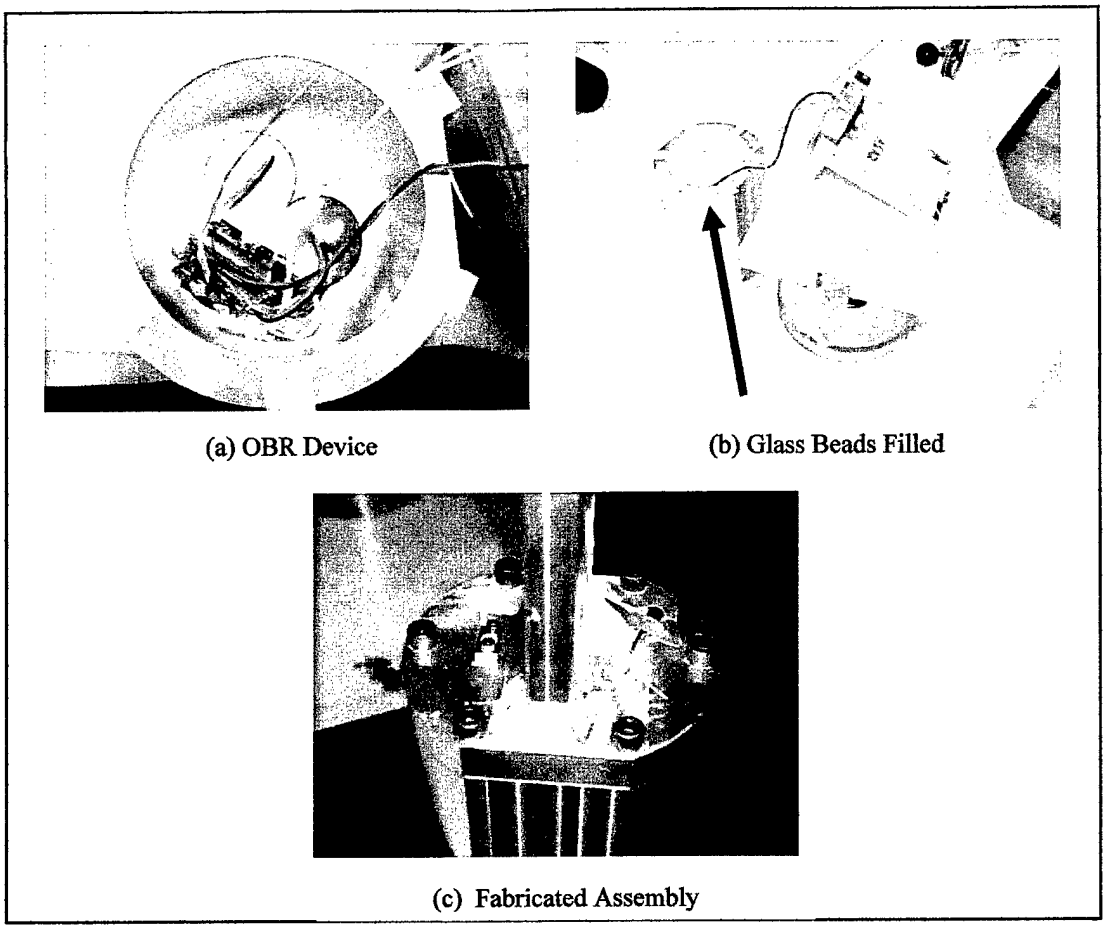

(a) OBR Device

(b) Glass Beads Filled

(c) Fabricated Assembly

Figure 6. OBR assembly process for the test projectile.

Table 1. Basic physical data for the air gun test.

Parameters	Shot 1	Shot 2	Shot 3
MEM weight, g	31,300	40,000	30,000
Instrumented bird weight, kg	3.25	3.25	3.25
Mitigator weight, g	1140	1200	1100
Mitigator material	7075-T6 A1	7075-T6 A1	7075-T6 A1
Mitigator diameter, in	3.87	3.85	3.9
Mitigator strength, lbf	102,317	100,463	90,347
Mitigator initial length, in	10.1	10.99	11
Mitigator crushed length, in	8.28	6.9	3.98
Wedge depth, in	1.5	1.5	1.5
No. of wedge peaks	2	2	2
Maximum acceleration, kg	~17	~18	~17
Posttest remarks	No damage to the catch tube	No damage	One of the 0.5-in tie rods broke, and the top-half of the catch tube flew away

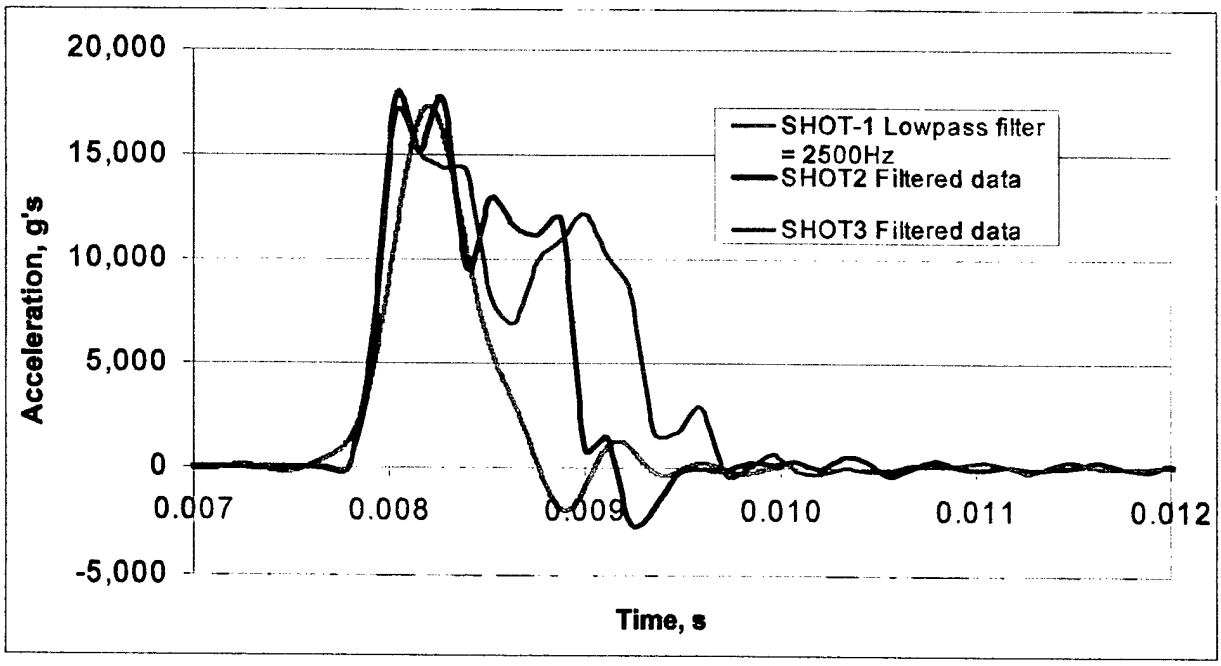

Figure 7. Air gun test results, top accelerations.

4.1 Material 126

This material model is suited to model metallic honeycomb (*2–4*). The behavior before compaction is orthotropic where the components of the stress tensor are uncoupled, i.e., a component of strain will generate resistance in the local a-direction with no coupling to the local b and c directions. The elastic modulii vary from their initial values to the fully compacted values linearly with the relative volume:

$$\begin{aligned} E_{aa} &= E_{aau} + \beta(E - E_{aau}) & G_{ab} &= G_{abu} + \beta(G - G_{abu}) \\ E_{bb} &= E_{bbu} + \beta(E - E_{bbu}) & G_{bc} &= G_{bcu} + \beta(G - G_{bcu}), \\ E_{cc} &= E_{ccu} + \beta(E - E_{ccu}) & G_{ca} &= G_{cau} + \beta(G - G_{cau}) \end{aligned} \tag{1}$$

where

$$\beta = \max\left[\min\left(\frac{1-V}{1-V_f}, 1\right), 0\right] \tag{2}$$

and G is the elastic shear modulus for the fully compacted honeycomb material:

$$G = \frac{E}{2(1+\nu)}. \tag{3}$$

The relative volume, V, is defined as the ratio of the current volume over the initial volume, and typically, $V = 1$ at the beginning of a calculation.

At the beginning of the stress update, we transform each element's stresses and strain rates into the local element coordinate system. For the uncompacted material, the stress components are updated using the elastic interpolated modulii according to the following:

$$\begin{aligned} \sigma_{aa}^{n+1_{trial}} &= \sigma_{aa}^{n} + E_{aa}\Delta\varepsilon_{aa} & \sigma_{ab}^{n+1_{trial}} &= \sigma_{ab}^{n} + E_{ab}\Delta\varepsilon_{ab} \\ \sigma_{bb}^{n+1_{trial}} &= \sigma_{bb}^{n} + E_{bb}\Delta\varepsilon_{bb} & \sigma_{bc}^{n+1_{trial}} &= \sigma_{bc}^{n} + E_{bc}\Delta\varepsilon_{bc} \\ \sigma_{cc}^{n+1_{trial}} &= \sigma_{cc}^{n} + E_{cc}\Delta\varepsilon_{cc} & \sigma_{ca}^{n+1_{trial}} &= \sigma_{ca}^{n} + E_{ca}\Delta\varepsilon_{ca} \end{aligned} . \quad (4)$$

We then independently check each component of the updated stresses to ensure that they do not exceed the permissible values determined from the load curves, e.g., if

$$\left|\sigma_{ij}^{n+1_{trial}}\right| > \lambda\sigma_{ij}\left(\varepsilon_{ij}\right) \quad (5)$$

then

$$\sigma_{ij}^{n+1} = \sigma_{ij}\left(\varepsilon_{ij}\right)\frac{\lambda\sigma_{ij}^{n+1_{trial}}}{\left|\sigma_{ij}^{n+1_{trial}}\right|} . \quad (6)$$

The components of $\sigma_{ij}\left(\varepsilon_{ij}\right)$ are defined by load curves.

The material model requires the stress vs. strain curve to be supplied. The strain for this material model must be input as logarithmic strain (*5*). Therefore, the experimental data which are given in terms of engineering strain must be converted. The relation between the engineering strain, e, and the logarithmic strain, ε, is as follows:

$$\varepsilon = ln(1+e) = ln(\left|\frac{L}{L_o}\right|) , \quad (7)$$

where the engineering strain, e, is defined by the following equation:

$$e = \frac{L-L_o}{L_o} = \frac{L}{L_o} - 1 = \frac{\Delta L}{L_o} . \quad (8)$$

For instance, if the efficiency of the honeycomb material is 90%, the material final length is only 10% of its initial length. The logarithmic strain in this case is

$$\varepsilon = \left|ln(\left|\frac{0.1}{1.0}\right|)\right| = 2.3026 . \quad (9)$$

4.2 Material 63

This material model is suited for modeling crushable foam (*2–4*). This isotropic foam model crushes one-dimensionally with a Poisson's ratio that is essentially zero. In the implementation, we assume that Young's modulus is constant and update the stress assuming elastic behavior:

$$\sigma_{ij}^{n+1_{trial}} = \sigma_{ij}^{n} + E\dot{\varepsilon}_{ij}^{n+1/2}\Delta t^{n+1/2}. \tag{10}$$

The magnitudes of the principal values σ_i^{trial}, $i = 1,3$ are then checked to see if the yield stress σ_y is exceeded; if so, they are scaled back to the yield surfaces such that if

$$\sigma_y < \left|\sigma_i^{trial}\right| \tag{11}$$

then

$$\sigma_{ij}^{n+1} = \sigma_y \frac{\sigma_i^{trial}}{|\sigma_i^{trial}|}. \tag{12}$$

After the principal values are scaled, the stress tensor is transformed back into the global system.

The material model requires the stress vs. strain curve to be supplied. The strain for this material model must be input as volumetric strain (*5*). Therefore, the experimental data which are given in terms of engineering strain must be converted. The volumetric strain, ε_v, is defined as follows:

$$\varepsilon_v = 1 - \frac{V}{V_o} = 1 - \frac{AL}{A_o L_o}. \tag{13}$$

Since we can assume that the crushable foam is crushed under a very small Poisson's ratio, the initial cross-sectional area is the same as the final one. Therefore, in this case the volumetric strain can be simplified as follows:

$$\varepsilon_v = 1 - \frac{L}{L_o}. \tag{14}$$

For instance, if the efficiency of the honeycomb material is 90%, the material final length is only 10% of its initial length. The volumetric strain in this case is

$$\varepsilon_v = 1 - \frac{L}{L_o} = 1 - \frac{0.1}{1.0} = 0.90. \tag{15}$$

4.3 Material Parameters

Mechanical compressive load carrying behavior for an Al mitigator can be described using the normalized load-deflection profile shown in Figure 8. As seen in the figure, three distinct features characterize the honeycomb mitigator's load carrying behavior. These features include linear elastic tendency up to initial crushing, typical volumetric crush, and final phase hardening

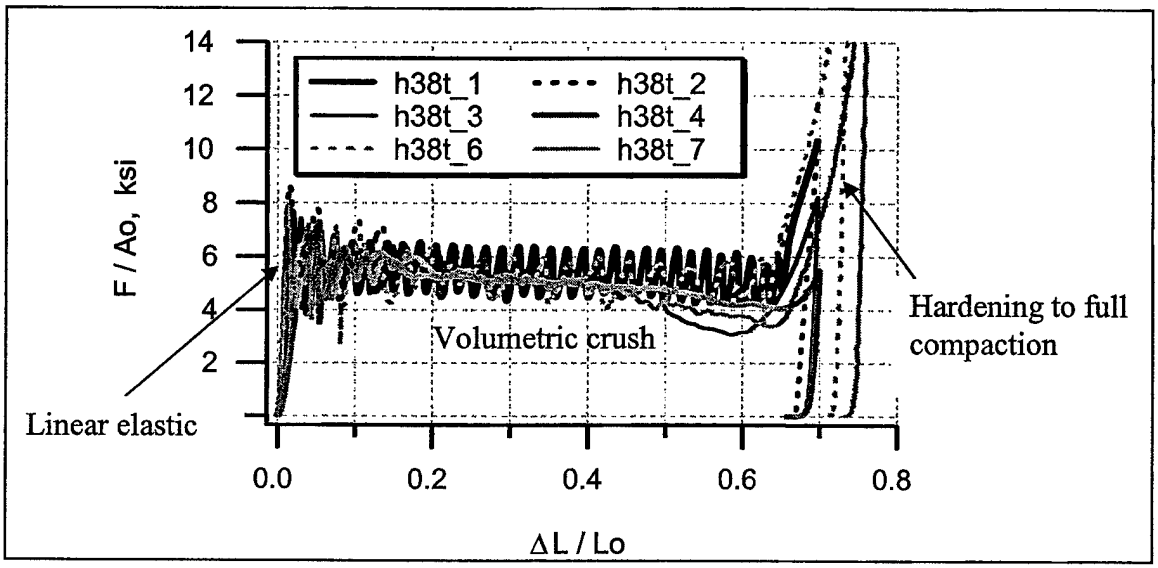

Figure 8. Normalized load-displacement of Hexcel 38 pcf compressed statically in the axial direction (*1*).

to full compaction. Almost all energy absorption is done in the volumetric crush zone. Initial spikes at the end of linear behavior are typical in Al honeycomb resistance profile and can be eliminated by crushing the striking edge of the mitigator. The fluctuation of strength during volumetric crushing, as seen in the figure, may have resulted by instability due to buckling of honeycomb cells.

Six honeycomb specimens (Hexcel 38 pcf) were tested statically by Lu and Hinnerichs (*1*). Compression tests for these specimens were performed along the principal material direction. Figure 8 shows the compression results. A confined compression test was also conducted by Lu and Hinnerichs (*1*), and the results are depicted in Figure 9. The rate of loading used is 4267 mm/s (14 ft/s). The solid line in Figure 9 is the stress-strain curve obtained from the dynamic test while the dotted line represents the average behavior. In the figure, the three zones are clearly shown and are the ones used in determining the material parameters needed by materials 126 and 63 in LS-DYNA.

Material parameters that are needed for FE material models are derived from the load-displacement curve described in Figure 8. The dynamic crush strength, however, increases with higher impact velocity, which must be accounted for in the material formulation (*6*). Parameters of interest for the material model include the following: crush strength, crush efficiency (volumetric strain that initiates the hardening), hardening modulus, and strain rate enhancement due to increase in impact velocity. In this investigation, a stress scale factor (relative increase in strength due to impact velocity) is used because of the unavailability of high strain rate dependent experimental data. A range of stress scale factor, suggested by Bitzer (*6*), is studied to determine the sensitivity of such parameters in governing the dynamics of the projectile model.

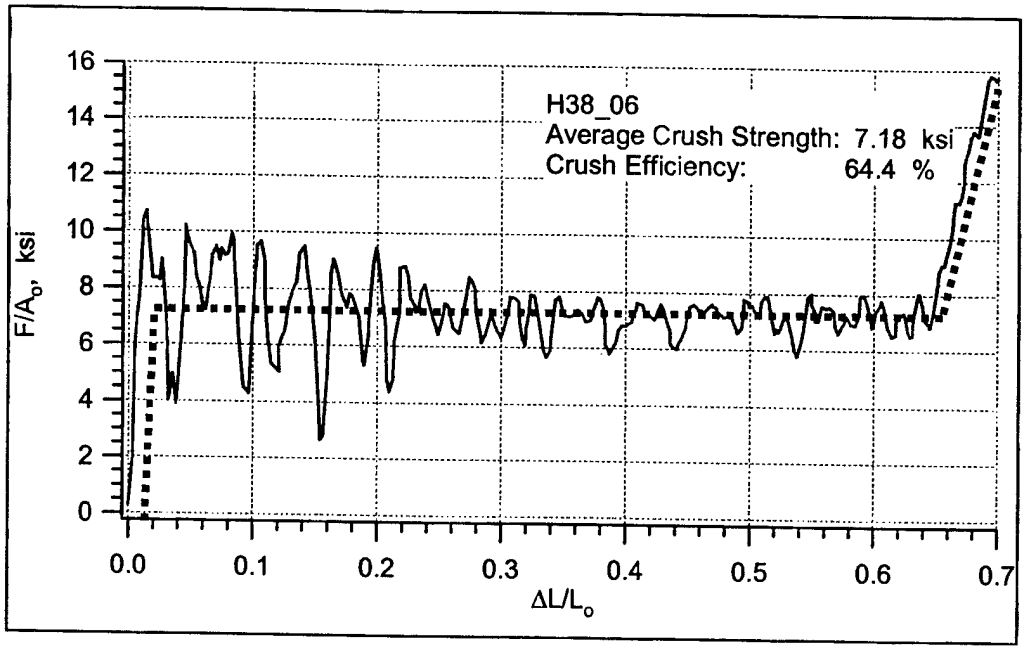

Figure 9. A confined high strain rate test of the Hexcel 38 14 ft/s in the axial direction (*1*).

Figures 10 and 11 report the material parameters extracted from the tests and used in LS-DYNA's *MAT_MODIFIED_HONEYCOMB and *MAT_CRUSHABLE_FOAM material, respectively. Two sets of load curves are used in the material models. One is for 90% compaction and the other is for 64% compaction. Lu and Hinnerichs (*1*) report that the material efficiency is 64% and full compaction is at 78%.

In order to verify the validity of the previously mentioned materials models, an FE model was developed to simulate the compression test reported by Lu and Hinnerichs (*1*). The displacement control is used in the simulation. The stress-strain curve for the case of 90% compaction is shown in Figure 12 for both material models (126 and 63). A 90% efficiency means that the final length is only 10% of its initial length. Figure 13 depicts the stress-strain curves for the case of 64% compaction for both material models. Material 126 has a strain rate effect algorithm. The strain rate effect is activated by the seventh material parameter on the first control card in the material model. The strain rate parameter's function is to shift the stress value above the static values as determined by the material parameters in the material model. A simulation is performed in which the average strain rate is 50 mm/mm/s, and the strain rate parameter used in the model is 100. Figure 14 depicts the stress-strain curve for the static and rate sensitive cases. One can observe that for this case, the rate sensitive stress is about two times the static stress. This simulation testifies to the effectiveness of the proposed material models in simulating the mean load-displacement relationship of the Al honeycomb mitigator. This material model, however, disregards the strength fluctuation that exists in physical tests (see Figure 8).

```
$---+----1----+----2----+----3----+----4----+----5----+----6----+----7----+----8
*MAT_MODIFIED_HONEYCOMB
       2 1.000E-10 4.060E+03    0.0000 5.588E+01 1.000E-03    1.0e-9
     66.0      66.0      66.0      66.0       0.0       0.0       0.0       0.0
   4060.00   4060.00   4060.00    2028.0    2028.0    2028.0       0.0
 0.000E+00     0.000E+00     0.000E+00     0.000E+00     0.000E+00     0.000E+00
 0.000E+00       0.000E+00       0.000E+00       0.000E+00       0.000E+00       0.000E+00
0.000E+00
*DEFINE_CURVE
      66
     0.00500000E+00      13.750
     0.02000000E+00      55.160
     2.3026            60.000
     3.00000           40.60e2
*DEFINE_CURVE
      661
     0.00500000E+00      13.750
     0.02000000E+00      55.160
     1.02170           60.000
     3.00000           40.60e2
$---+----1----+----2----+----3----+----4----+----5----+----6----+----7----+----8
```

Figure 10. Material 126 input parameters.

```
$---+----1----+----2----+----3----+----4----+----5----+----6----+----7----+----8
*MAT_CRUSHABLE_FOAM
       1   1.0E-10   4060.00     0.000       67            1.0e-9
*DEFINE_CURVE
      671
     0.00500000E+00      13.750
     0.02000000E+00      55.160
     0.90              60.000
     0.99000000E+00      40.60e2
*DEFINE_CURVE
      67
     0.00500000E+00      13.750
     0.02000000E+00      55.160
     0.64              60.000
     0.99000000E+00      40.60e2
$---+----1----+----2----+----3----+----4----+----5----+----6----+----7----+----8
```

Figure 11. Material 63 input parameters.

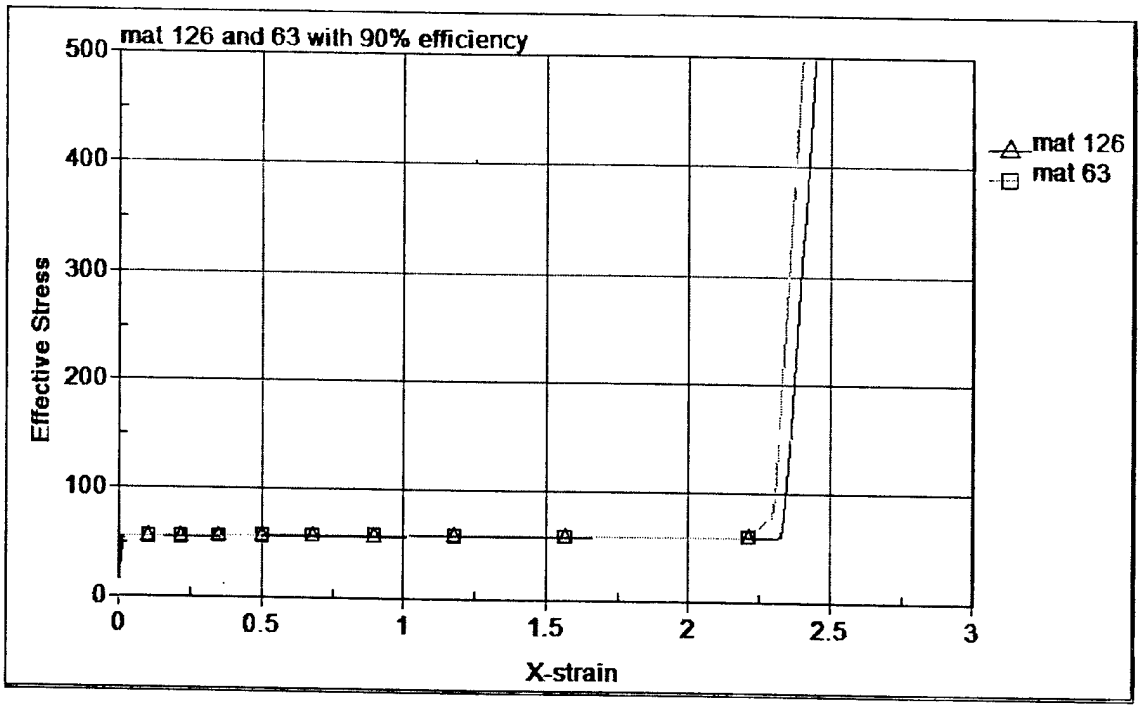

Figure 12. Stress-strain curves for materials 126 and 63, 90% compaction.

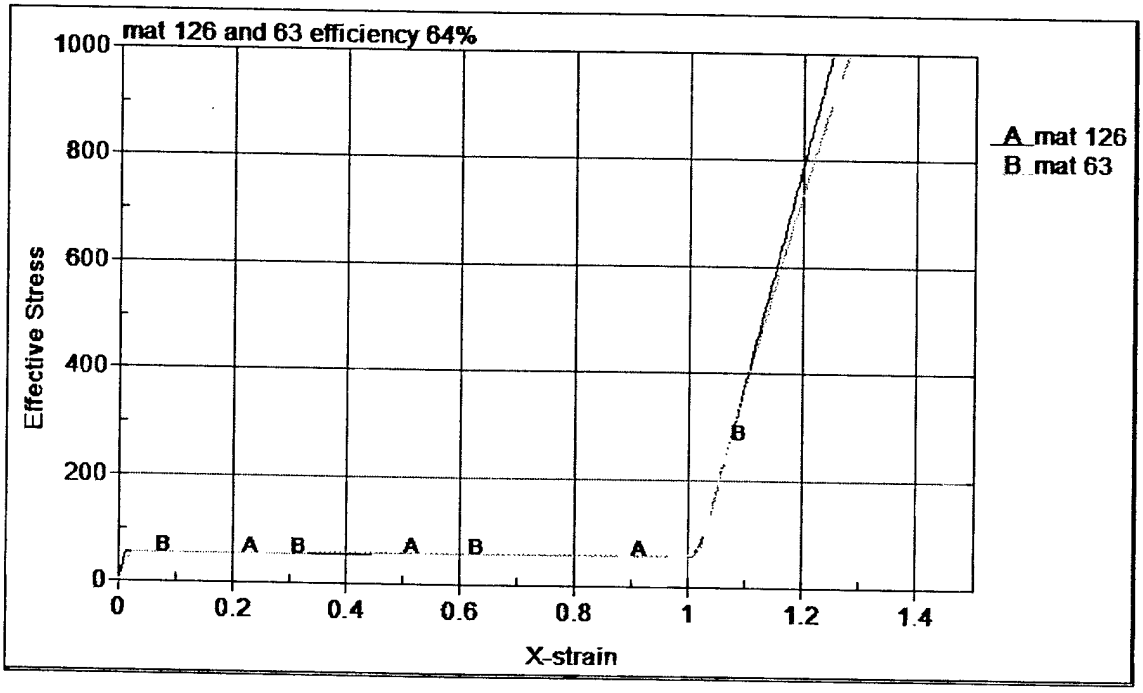

Figure 13. Stress-strain curves for materials 126 and 63, 64% compaction.

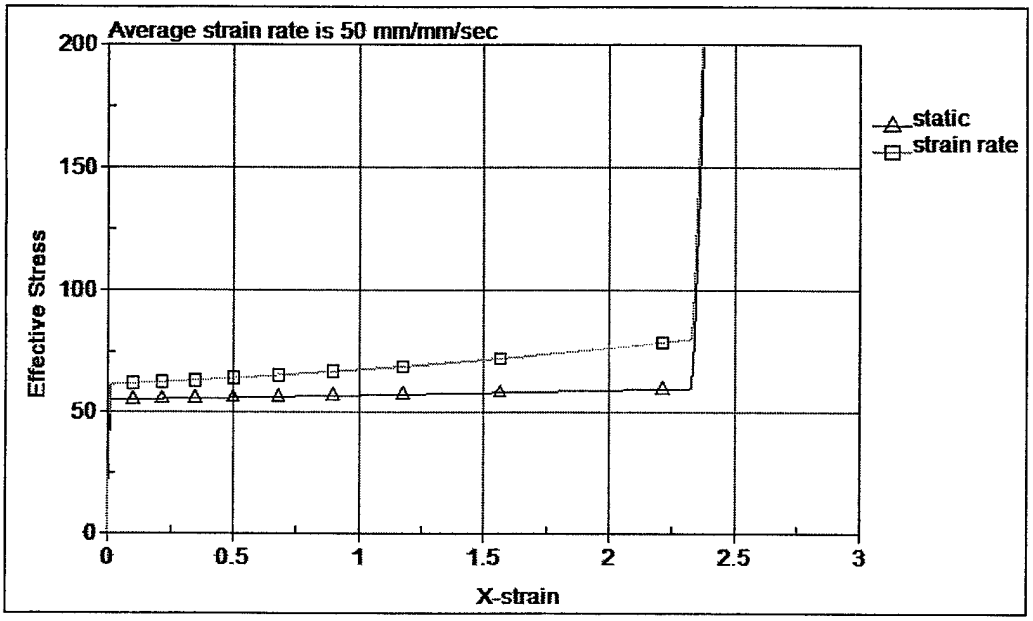

Figure 14. Stress-strain curves for material 126 with strain rate effect.

5. The FE Model

Four FE models were developed in this investigation. Two models are used in the Lagrangian simulations and two are used in the ALE simulations. The two sets are coarse and fine mesh. The two simulation methods are used and considered since it is anticipated that the Lagrangian simulation is unstable due to large deformation of the Al honeycomb. Lagrangian descriptions of material have limitations for severe mesh distortion. On the other hand, the Eulerian description of material is more stable under large deformation since the material is assumed to behave like fluid. In the next sections, a description of the two methods are presented in detail. Sample statistics on the Lagrangian and ALE methods are shown in Table 2. The statistics shown in this table are for computer runs that were conducted on an ARL high performance computer SGI Origin 2000* server system.

Table 2. Sample statistics of ALE (coarse mesh) and Lagrangian (fine mesh) models.

Parameter	FE Model	
	ALE	Lagrangian
No. of nodes	69,578	118,842
No. of elements (brick, beam, and shell)	65,724	123,164
Total execution time, ms	5	3.5
Time step, s	8.29e-8 to 1.20e-7	1.90e-7 to 1.72e7
CPU time, s	262,292	43,408

* SGI Origin 2000 is a registered trademark of Silicon Graphics Inc.

5.1 Lagrangian Model

The FE model of the Lagrangian test setup is depicted in Figure 15. The model consists of the catch tube (wired mesh), the OBR (brown mesh), the instrumented plate (dark blue mesh), the MEM (yellow mesh at the rear end), and four beam elements that represent the bolts connecting the two halves of the catch tubes. On modeling the OBR, no inner filler materials including the recording devices and the glass beads (Figure 6) were included in the FE model. The total mass of the instrumented OBR was simulated in the FE model by adjusting the density of the OBR canister. The analytic simulation of the impact starts with an initial input velocity for the projectile from the position shown in the figure. The initial velocity was obtained by double integrating the recorded accelerometer data from the actual test shot. As seen in the figure, the initial velocity of the projectile at its impact was ~83,566 mm/s (3290 in/s).

The fine mesh model is used for generation of the simulation results and the experimental comparison. The fine mesh model consists of 118,842 nodes and 123,164 elements. There are 14,744 shell elements, 108,416 solid elements, and 4 beam elements in the model. Several contact surfaces are defined in this model. A contact surface is defined between the OBR and the mitigator, the OBR and the catch tube, the mitigator and the catch tube, and the mitigator and the MEM. The segment-based contact is used in this case, which proved to be more stable. Two material models in the LS-DYNA simulation code are considered in this model: *MAT_MODIFIED_HONEYCOMB and *MAT_CRUSHABLE_FOAM.

5.2 ALE Model

Since it is difficult to simulate very large deformation in the Lagrangian method easily, the ALE method is employed. The Lagrangian method requires significant expertise in modeling severe deformation. The ALE method, on the other hand, is more stable for such problems. Two models are developed here as well: a coarse and a fine mesh. The coarse mesh model is employed for generation of the simulation results. The fine mesh model led to a very small time step which rendered the simulation computationally inefficient. The coarse mesh model consisted of 69,578 nodes and 65,724 elements. There are 4440 shell elements, 61,280 solid elements, and 4 beam elements in the model. The ALE finite element model is depicted in Figure 16. The model consists of the catch tube, the OBR (glass beads are not modeled as in Lagrangian case), the instrumented plate, and the MEM that is similar to the Lagrangian model. The mitigator, however, is modeled differently here. The mitigator is a model with solid element formulation no. 12 in LS-DYNA. This element formulation is ALE plus void, where the void is the surrounding space in which the distorted material can flow. The mesh in this part does not distort, which is the case with the Eulerian description of motion. The mitigator is surrounded by void elements. The void element is there for the possibility of the mitigator material flow. The mitigator material upon deformation can flow outside of the mitigator mesh. Once this happens, the mitigator material can flow into the void elements. The solid elements of the mitigator and

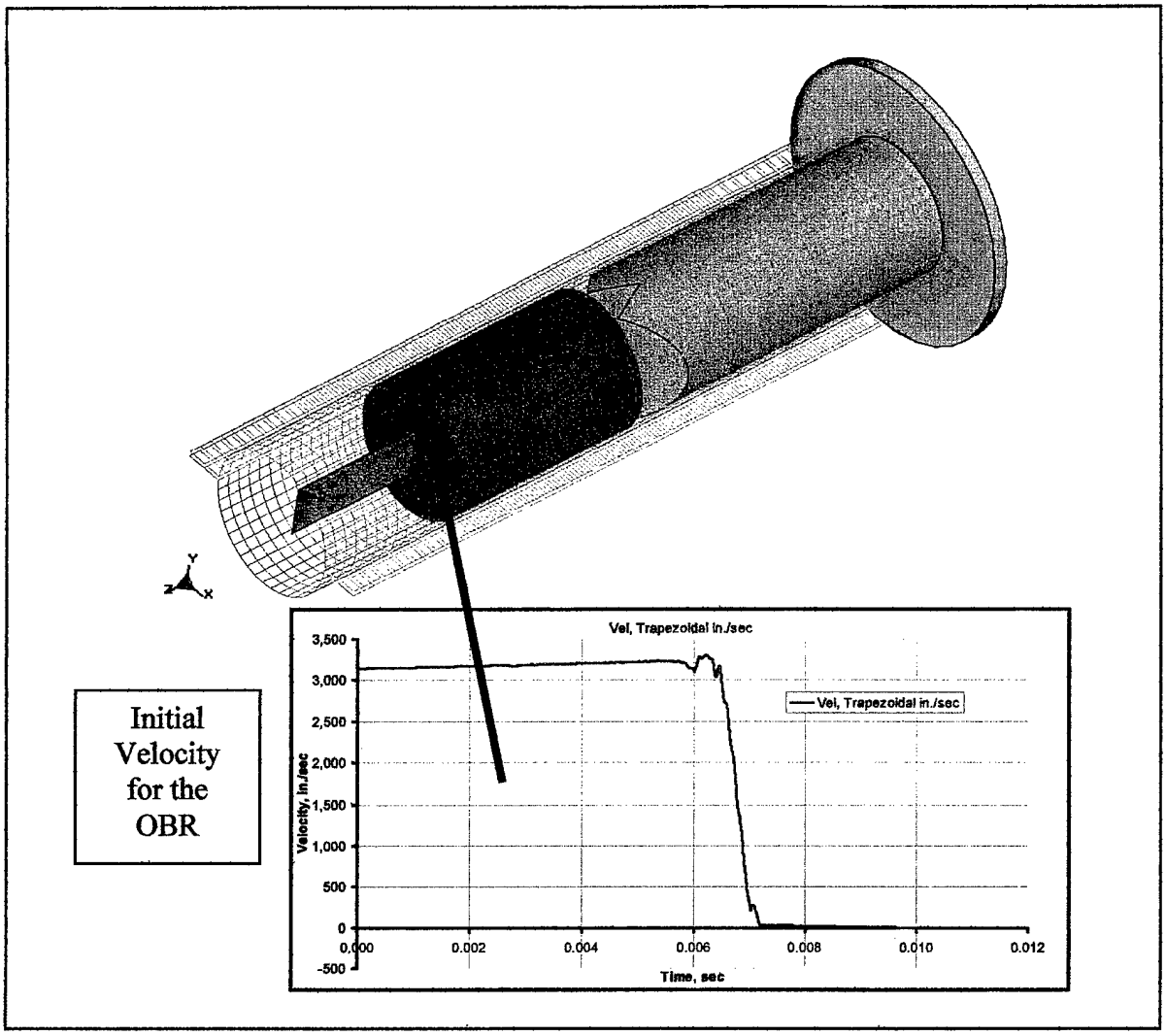

Figure 15. The Lagrangian FE model.

void have node-to-node correspondence at the boundaries. Figure 17 depicts a section cut through the middle of the mesh. The blue mesh in this figure represents the mitigator honeycomb; the red mesh is the surrounding void.

The integration time step in an ALE simulation is smaller than a Lagrangian simulation for the same mesh size. This is attributed to the way LS-DYNA does the ALE formulation. The explicit time integration time step in the Lagrangian method, in general, is a function of the smallest element's characteristic length and material properties. In the ALE method, in addition to that previously mentioned, it is also a function of mesh velocity, i.e., the velocity of the material grid as it distorts. Due to this fact, the integration time step in the ALE method is smaller than the Lagrangian method.

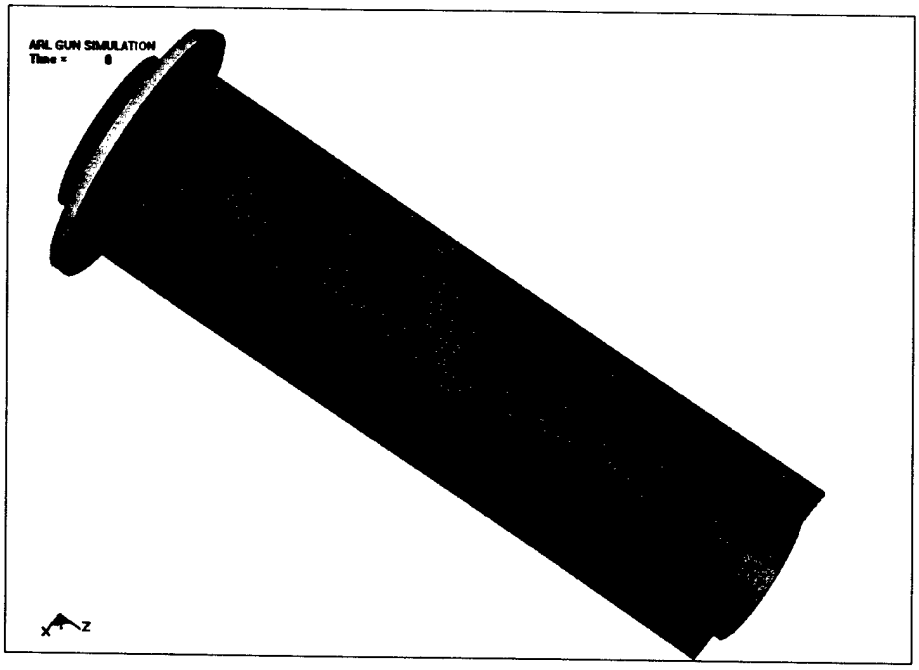

Figure 16. The ALE model.

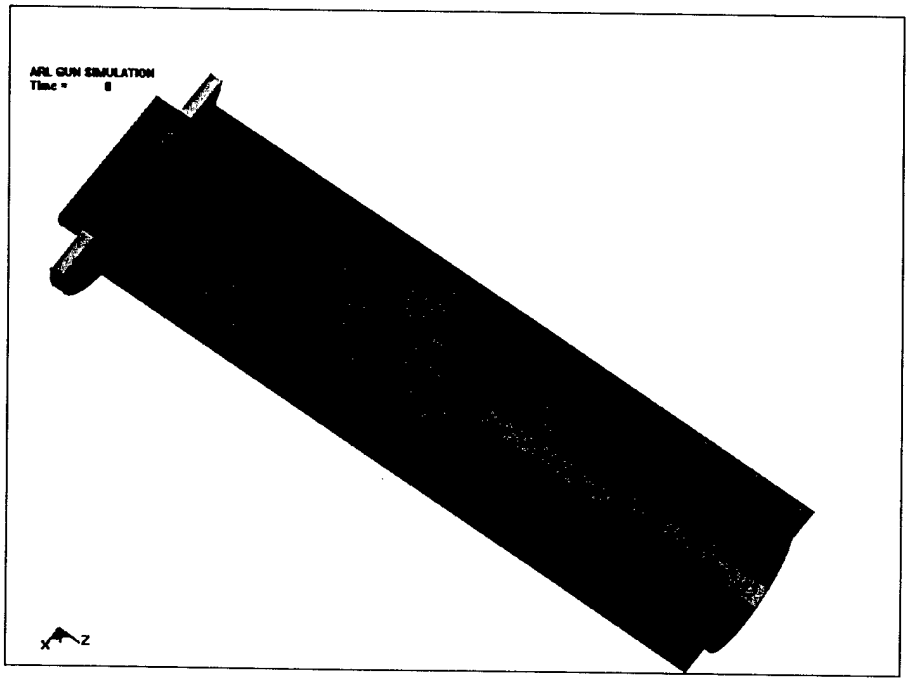

Figure 17. Section cut view of ALE model.

6. Simulation Results

The simulations were carried out on a 1.7-MHz laptop computer and also independently on an ARL Major Shared Resource Center (MSRC) SGI Origin 2000 server system. The duration of the impact event was ~2 ms. The contact of the OBR with the mitigator lasted only ~1 ms. Two types of simulations were carried out, namely, Lagrangian and Eulerian simulations. The CPU time using the laptop for the Lagrangian simulation was ~4 hr. The Eulerian simulation took ~16 hr to complete even though the number of elements is about one-half the Lagrangian simulation. The impact velocity in both models is taken as 83,566 mm/s. The three fundamental units used here are millimeters, seconds, and metric ton for the length, time, and density, respectively. Results of the two simulations are presented next.

6.1 Lagrangian Simulations

The Lagrangian simulation was carried out for two different material models in LS-DYNA: *MAT_MODIFIED_HONEYCOMB, which is material 126, and *MAT_CRUSHABLE_FOAM, which is material 63. Results of the simulations utilizing both material models are presented next.

6.1.1 Material 126

The material parameters used in this model are those listed in Figure 10. The stress values are scaled by 1.2 to account for the high-velocity impact. The strain rate effect must be included in such a simulation since the material exhibits strain rate sensitivity. However, since experimental data for the used honeycomb material under high strain rate are not available, the stresses are scaled by a multiplier. The range of stress scale factor used is between 1.2 and 1.5 for this material model (*6*).

Two different material efficiencies are considered for the simulations: 90% and 64% compaction. The 64% efficiency (or compaction) predicted a stiffer response than the 90% compaction. Figures 18–27 depict the simulation results for 90% efficiency. Figures 28 and 29 show the difference in predictions of the two efficiencies.

Figures 18 and 19 show the impacted geometry and closeup view of the impacted geometry for material 126, respectively. Figure 20 depicts the energy balance as predicted by the simulation. One can see that the energy is conserved in this simulation, which is an indication of numerical stability of the model. The hourglass energy and contact energy (not shown in the figure) is much smaller than the internal energy as desired in a stable impact simulation. The contact force between the OBR and the mitigator is shown in Figure 21. Figure 22 depicts the displacement of the MEM as a function of time.

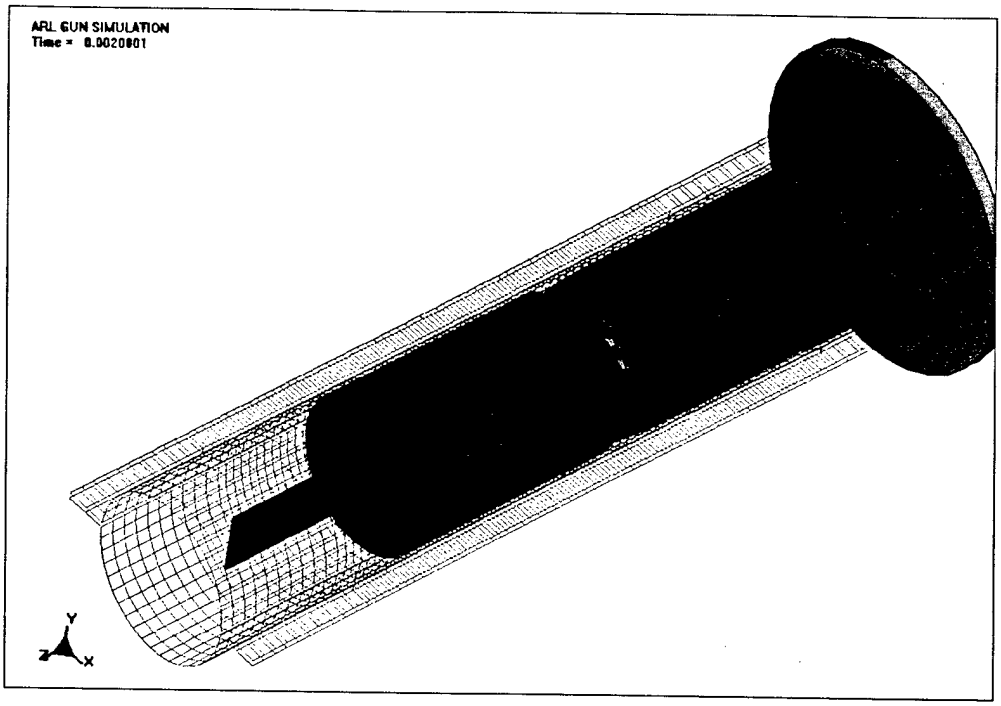

Figure 18. Material 126 impact simulation.

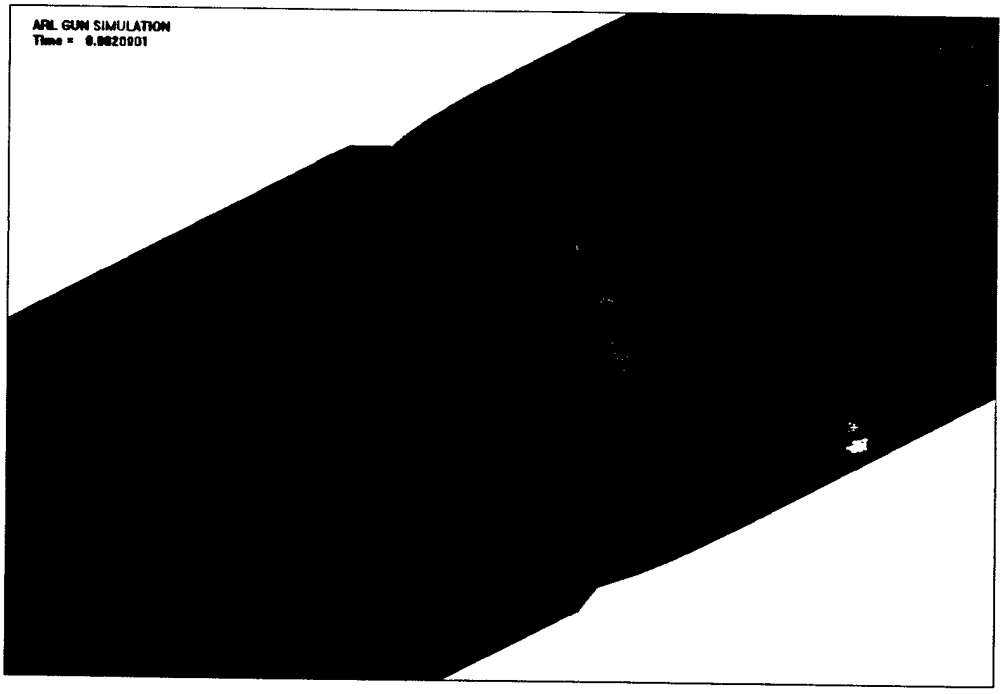

Figure 19. Material 126 impact simulation, closeup view.

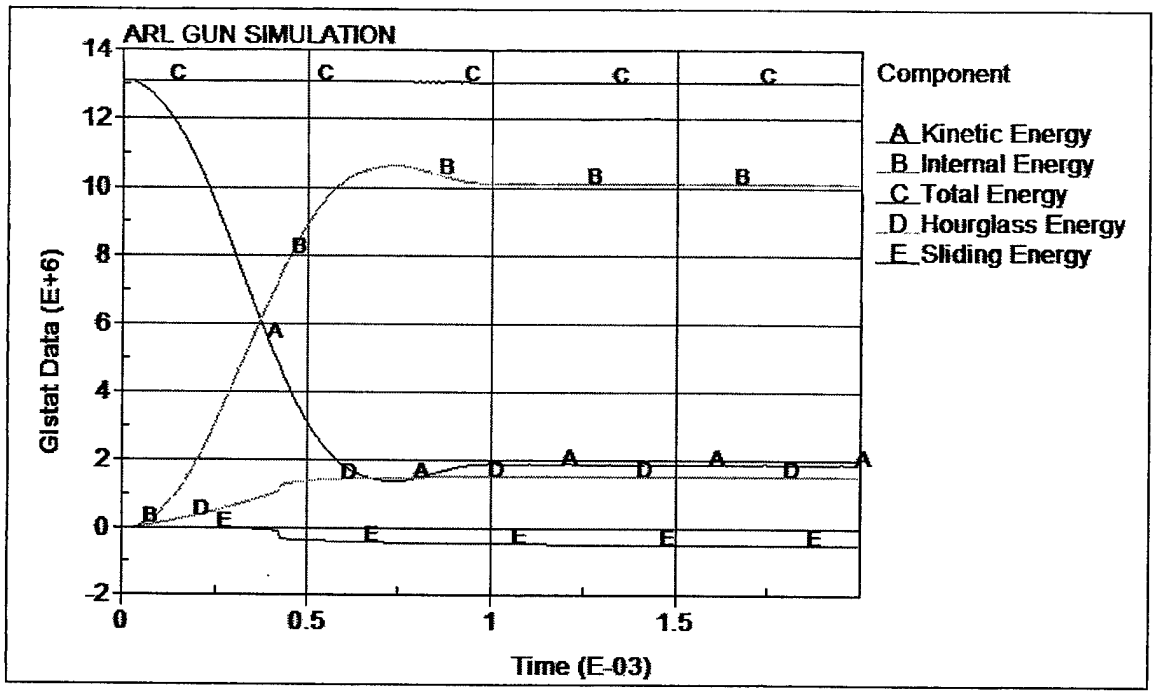

Figure 20. Energy balance, material 126.

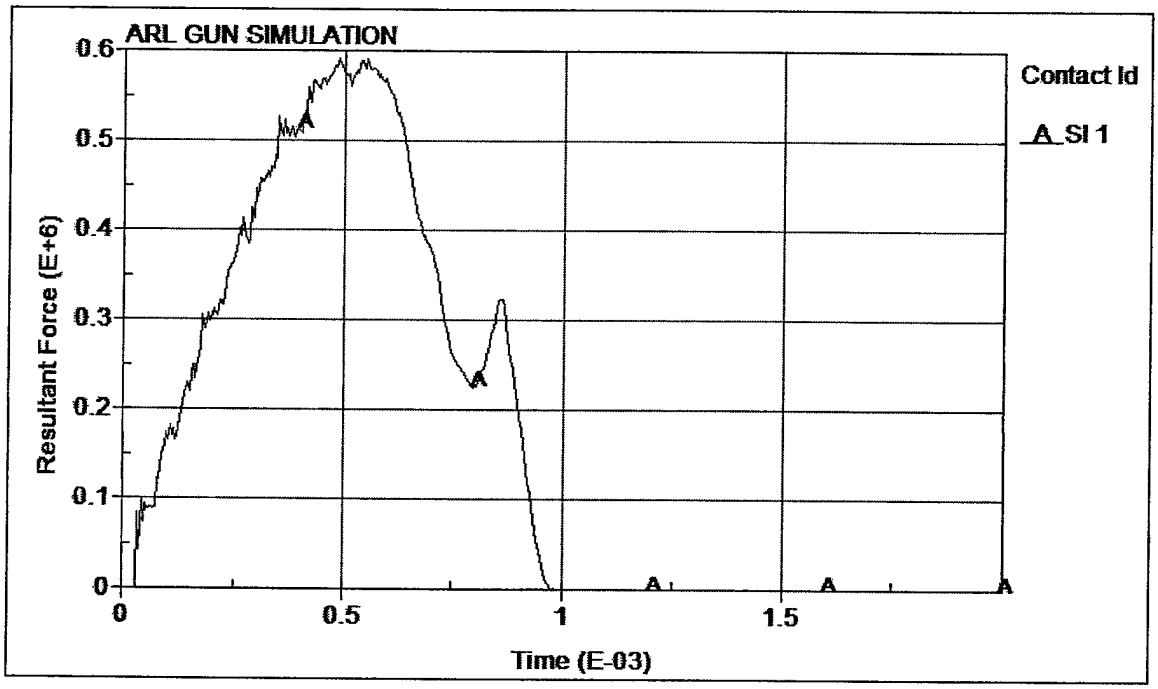

Figure 21. Contact force (OBR and mitigator), material 126.

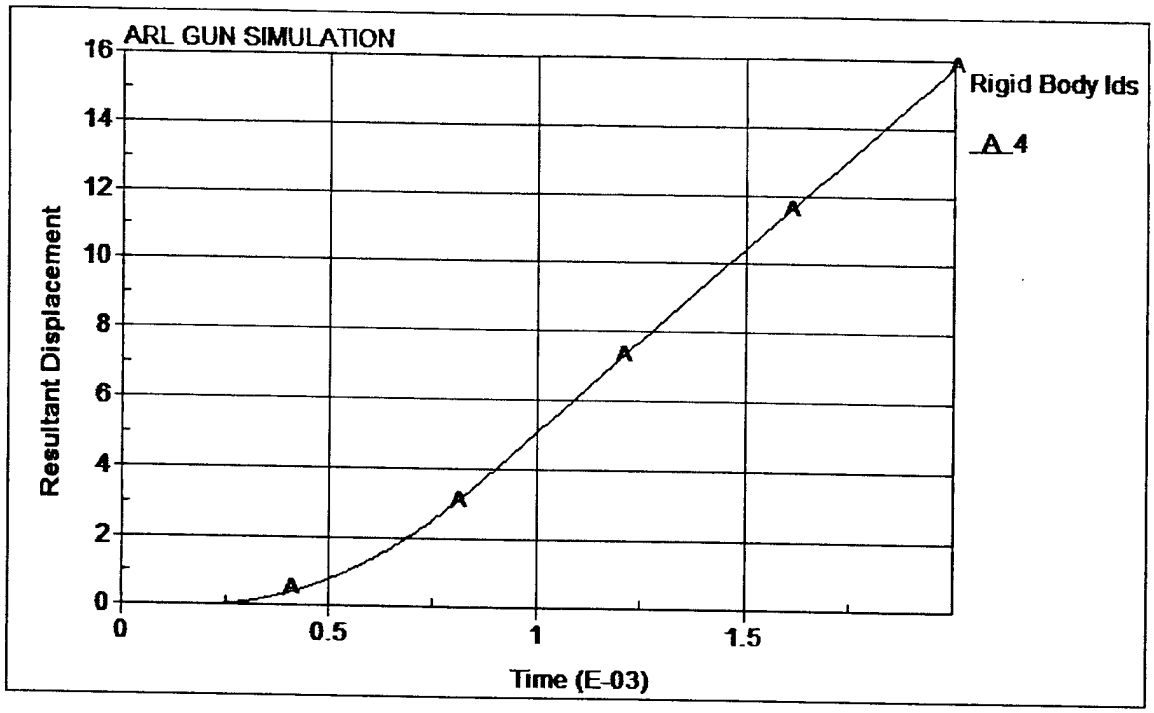

Figure 22. Displacement of the MEM, material 126.

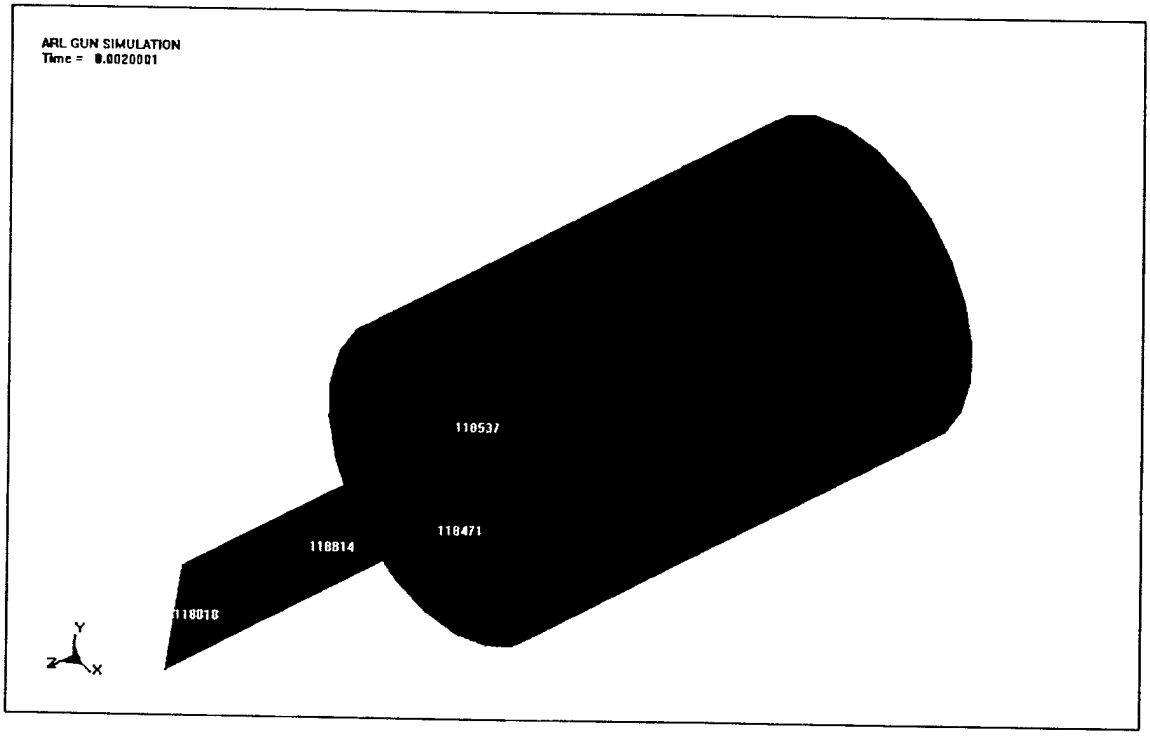

Figure 23. Nodal ID for velocity and acceleration output.

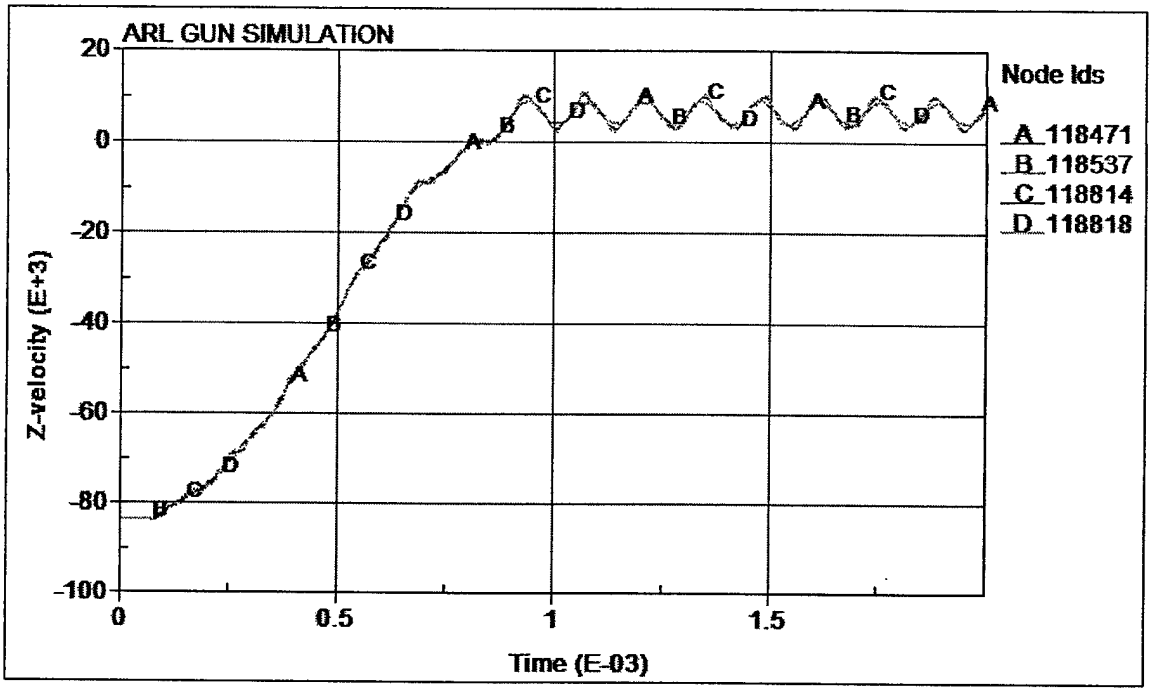

Figure 24. Velocity of OBR, material 126.

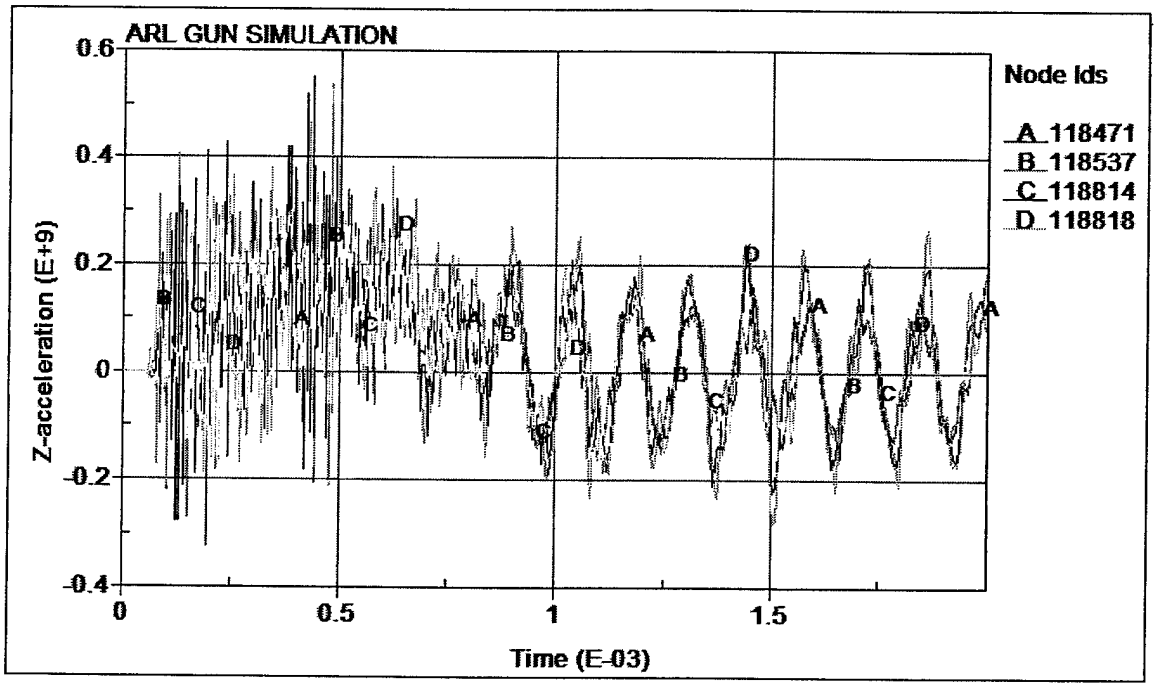

Figure 25. Acceleration of four nodes on the OBR, material 126.

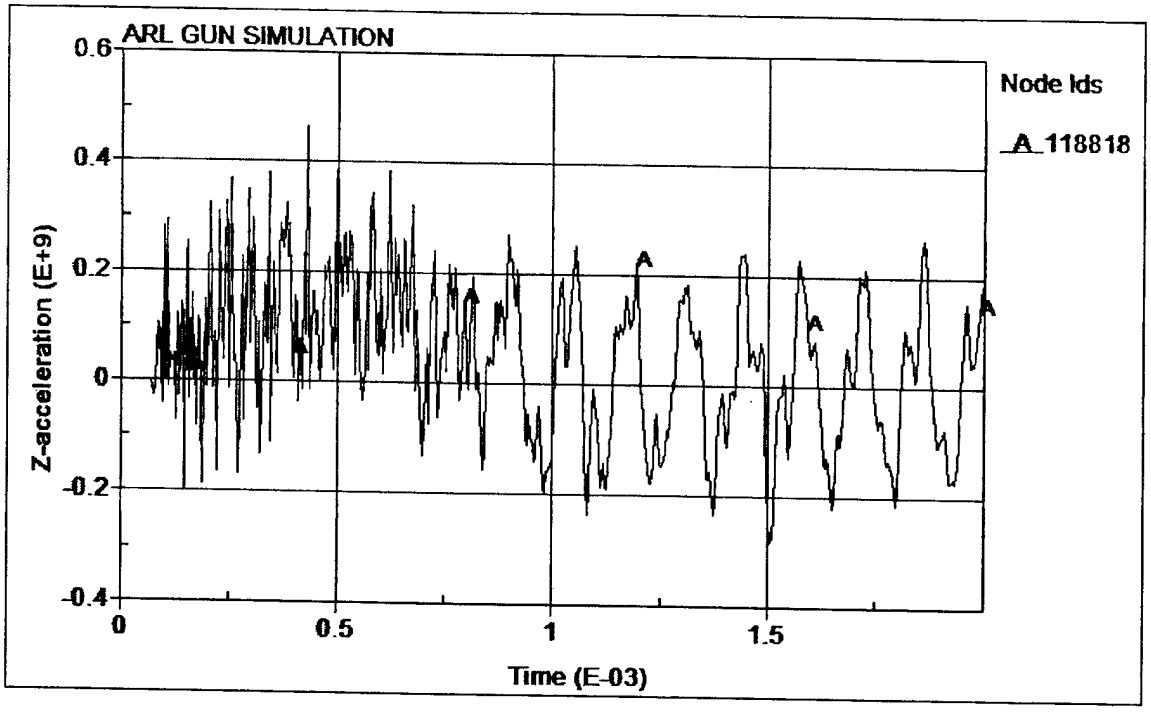

Figure 26. Acceleration of a top node on the OBR, material 126.

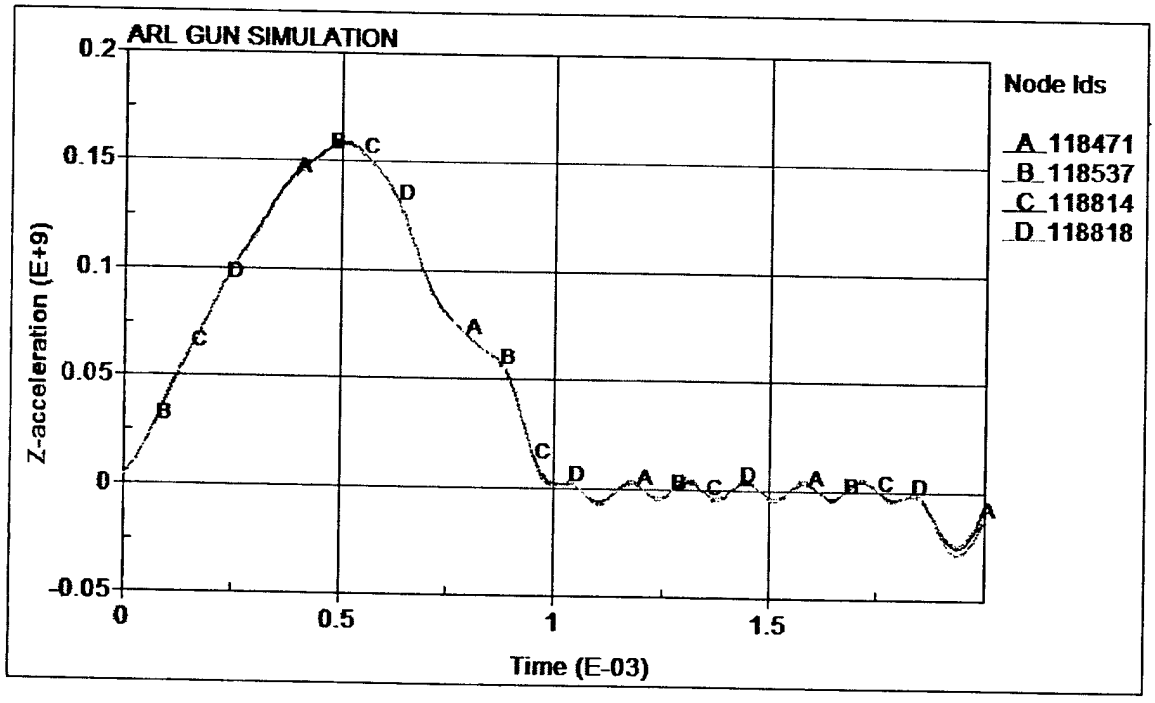

Figure 27. Acceleration of the top of the OBR filtered at 2500 Hz, material 126.

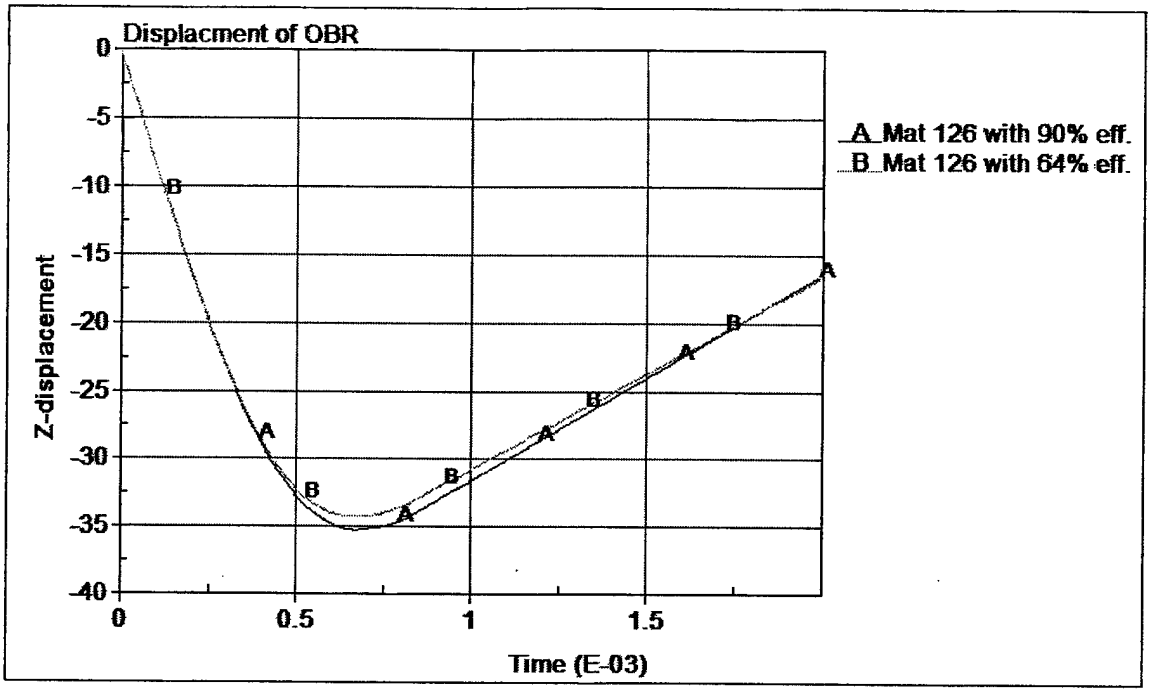

Figure 28. Displacement of the OBR for two different efficiencies of material 126.

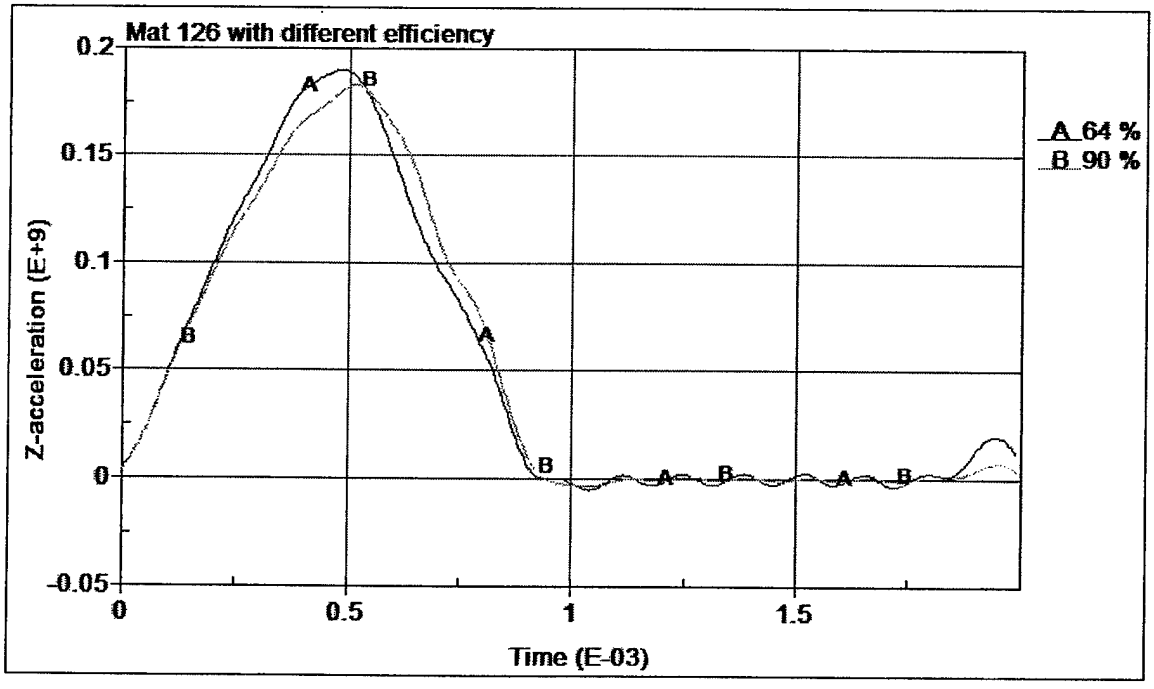

Figure 29. Acceleration of the top of the OBR for two different efficiencies of material 126.

To compare simulation responses to that of the experimental tests, several modal locations were selected for kinematics output. The locations of these nodes were the same locations on the OBR in the experimental tests. These locations are shown in Figure 23. The velocities of the selected nodes are shown in Figure 24. Figure 25 depicts the acceleration of these nodes. The frequency of output is selected to be the same as the one used in the experiments, which is 4.0E-6 s. The acceleration of the top of the OBR is shown in Figure 26. This acceleration data are filtered with a low-pass filter with a cutoff frequency of 2500 Hz and is shown in Figure 27.

The honeycomb material reported by Lu and Hinnerichs (*1*) has an efficiency of 64%–78%. The simulations indicated that the 64% efficiency model led to a stiffer behavior as far as the mitigator crushed distance is concerned. Figure 28 shows the displacement of the OBR for the two honeycomb efficiencies considered. One can observe that the 90% honeycomb efficiency led to more displacement of the OBR and consequently a greater crushed distance of the mitigator. The stress scale factors in these simulations were taken as 1.5. Figure 29 depicts the filtered acceleration of the top of the OBR for the two honeycomb efficiencies considered. These acceleration data are filtered with the same low-pass filter with a cutoff frequency of 2500 Hz.

6.1.2 Material 63

The *MAT_CRUSHABLE_FOAM in LS-DYNA is used in the following simulations. The stress is scaled by 1.5 to account for the strain rate sensitivity. The material input data for this simulation are reported in Figure 11.

The CPU time for the simulation using this material model is about the same as material model 126. The crushed mitigator is shown in Figure 30. The qualitative difference between the simulations using materials 63 and 126 was insignificant. Figure 31 depicts the velocity of the OBR as function of time. Figure 32 shows the acceleration of several nodes on the OBR. The frequency of output is the same as the previous material model and the same as the experimental data. The accelerations are filtered with a low-pass filter with a cutoff frequency of 2500 Hz and shown in Figure 33.

Figure 34 depicts the filtered acceleration of the top of the OBR for material 126 and material 63. The magnitude of the acceleration for the two materials is about the same. However, there is some difference in the duration of the pulse. This difference is attributed to the differences in the formulation of the two material models. The *MAT_MODIFIED_HONEYCOMB is an orthotropic material, which assumes that stress components are fully decoupled. Straining of the material in the local material axis in one direction causes stress in that direction only. However, the *MAT_CRUSHABLE_FOAM is an isotropic material model, and the stress components are not decoupled.

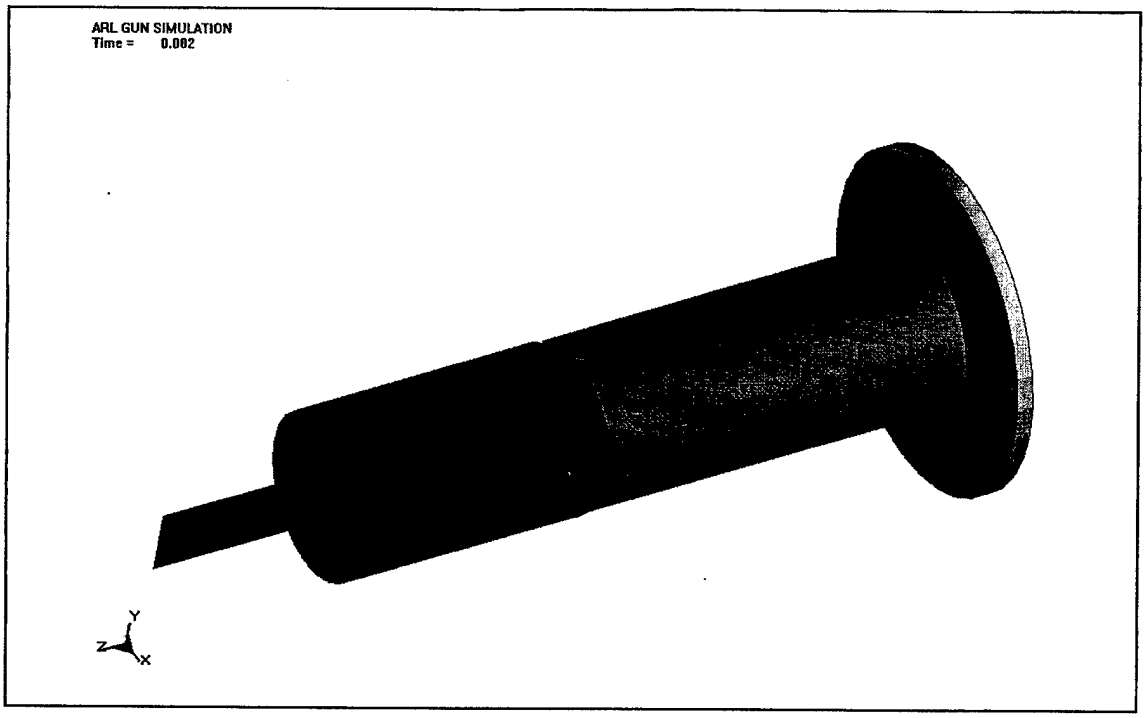

Figure 30. Crushed mitigator, material 63.

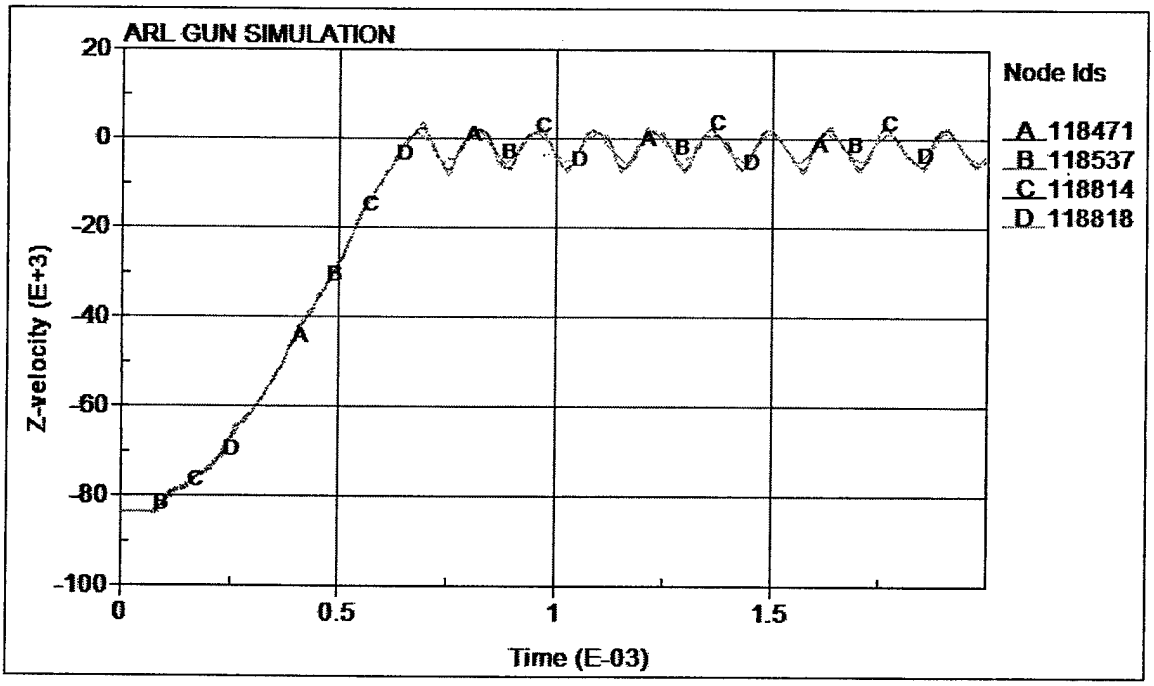

Figure 31. Velocity of several nodes on the OBR, material 63.

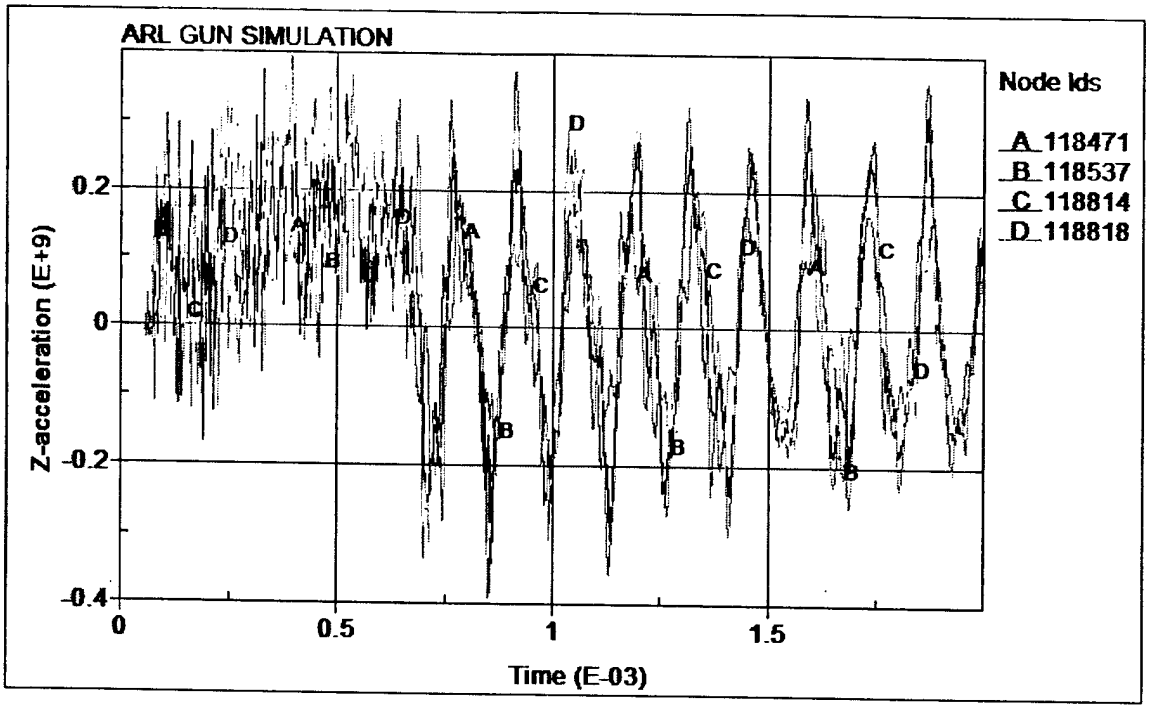

Figure 32. Acceleration of several nodes on the OBR, material 63.

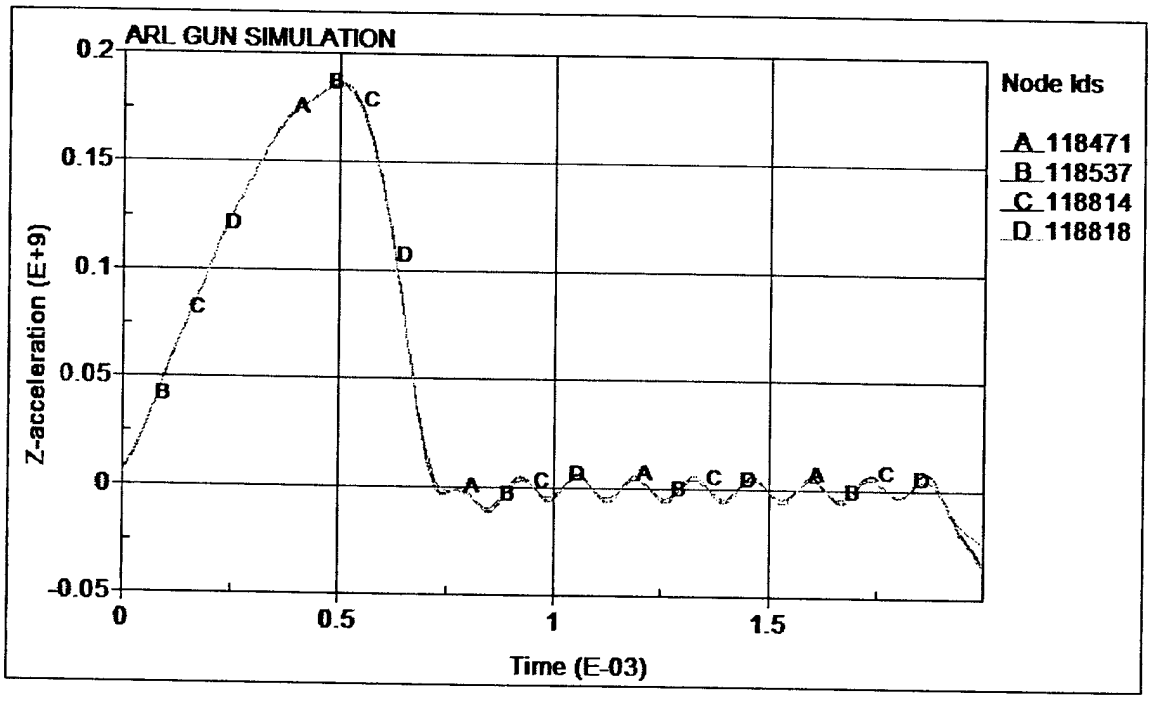

Figure 33. Acceleration of the top of the OBR filtered at 2500 Hz, material 63.

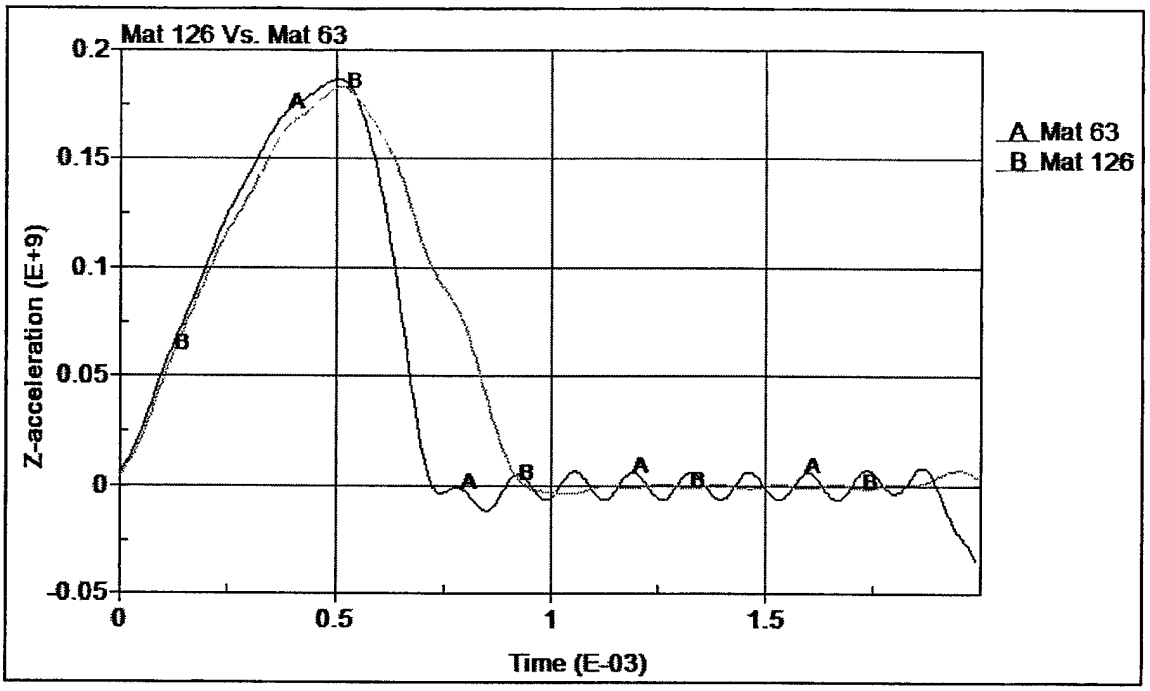

Figure 34. Acceleration of the top of the OBR using materials 126 and 63.

6.2 ALE Simulation

The mesh is fixed in an ALE simulation. In this situation, one can look at the volume fraction of the material. The volume fraction is equal to 1 when the element is filled with the material. Volume fraction <1 means that only part of the element is filled with the material. The volume fraction of the mitigator material at time zero is shown in Figure 35. The volume fraction of the mitigator material at the end of the simulation is depicted in Figure 36. One can observe that the Eulerian mesh has not moved; however, the material has passed from one element to the next indicating material flow and deformation.

Figure 37 shows locations of several nodal points for kinematics output. The velocity of the OBR as a function of time is shown in Figure 38. Acceleration of several nodes on the OBR is depicted in Figure 39. The frequency of output is selected to be the same frequency as in the experimental tests. The acceleration of the top of the OBR is depicted in Figure 40. These data are filtered with a low-pass filter with a cutoff frequency of 2500 Hz and are shown in Figure 41. Comparison of the prediction of the acceleration of the top of the OBR using the Lagrangian and ALE methods is shown in Figure 42. A small difference is observed in the magnitude of the peak acceleration. This difference, however, can be neglected and assumed to be a numerical error difference between the two methods.

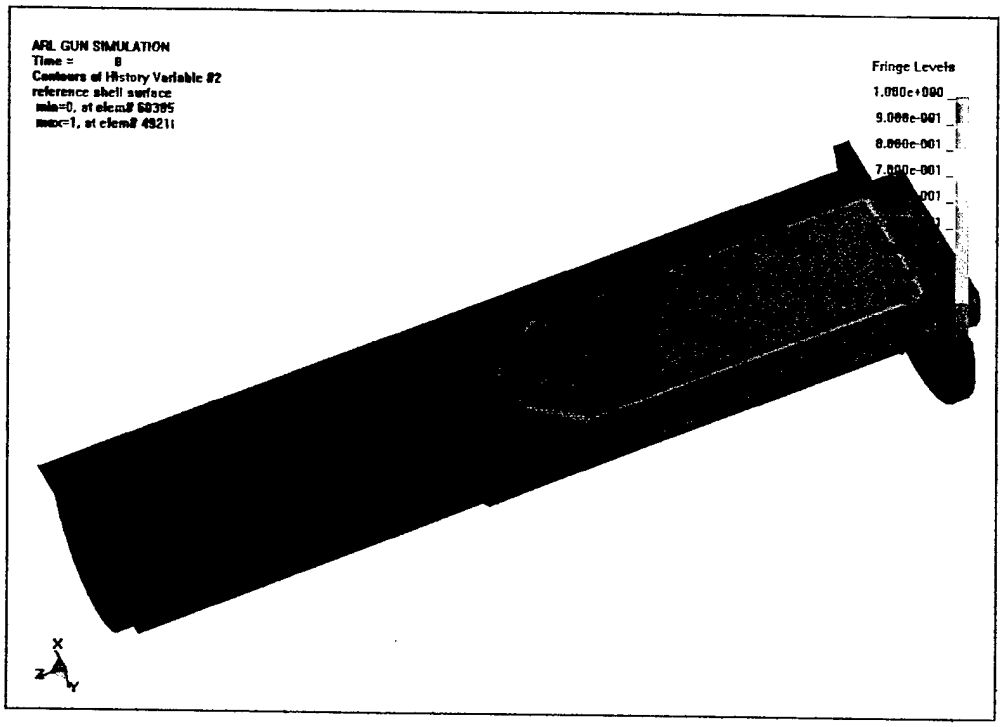

Figure 35. Volume fraction of the mitigator at time zero.

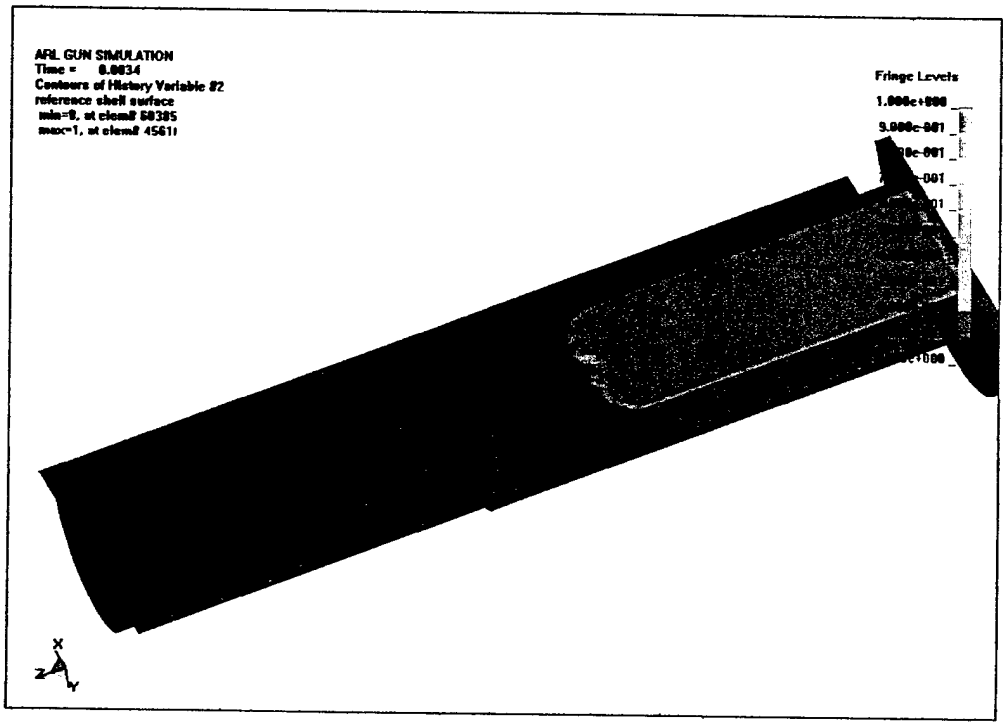

Figure 36. Volume fraction of the mitigator at the end of the simulation.

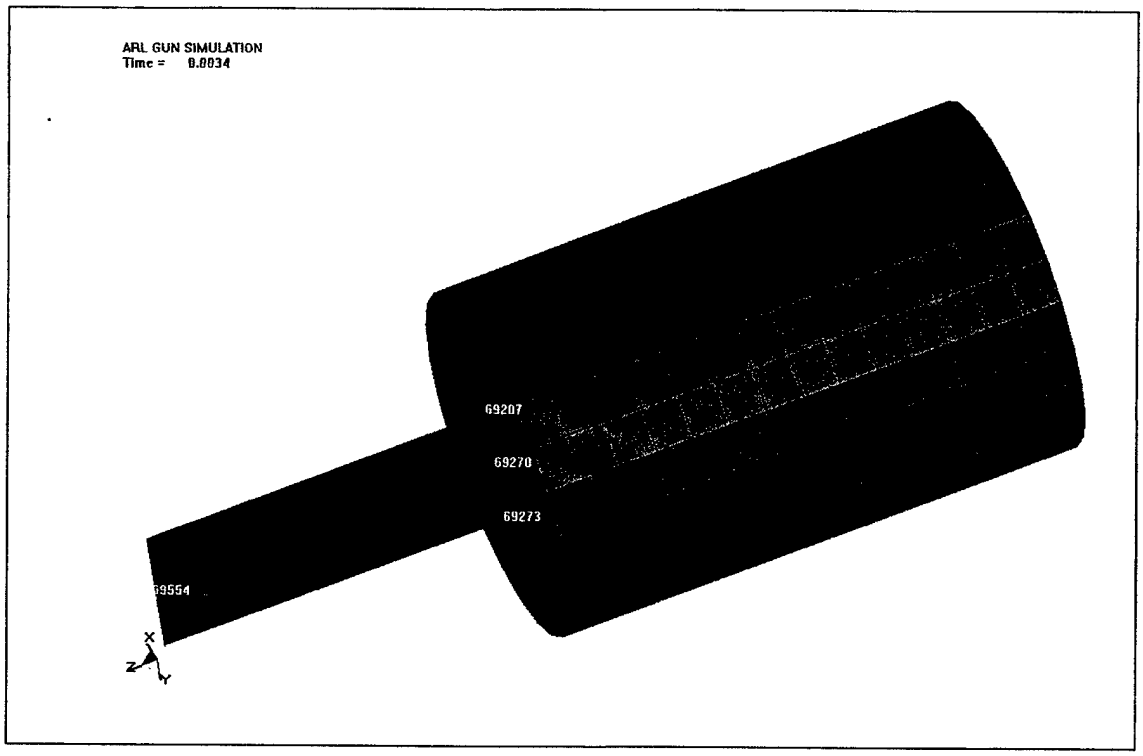

Figure 37. Locations of the nodal point for kinematics output.

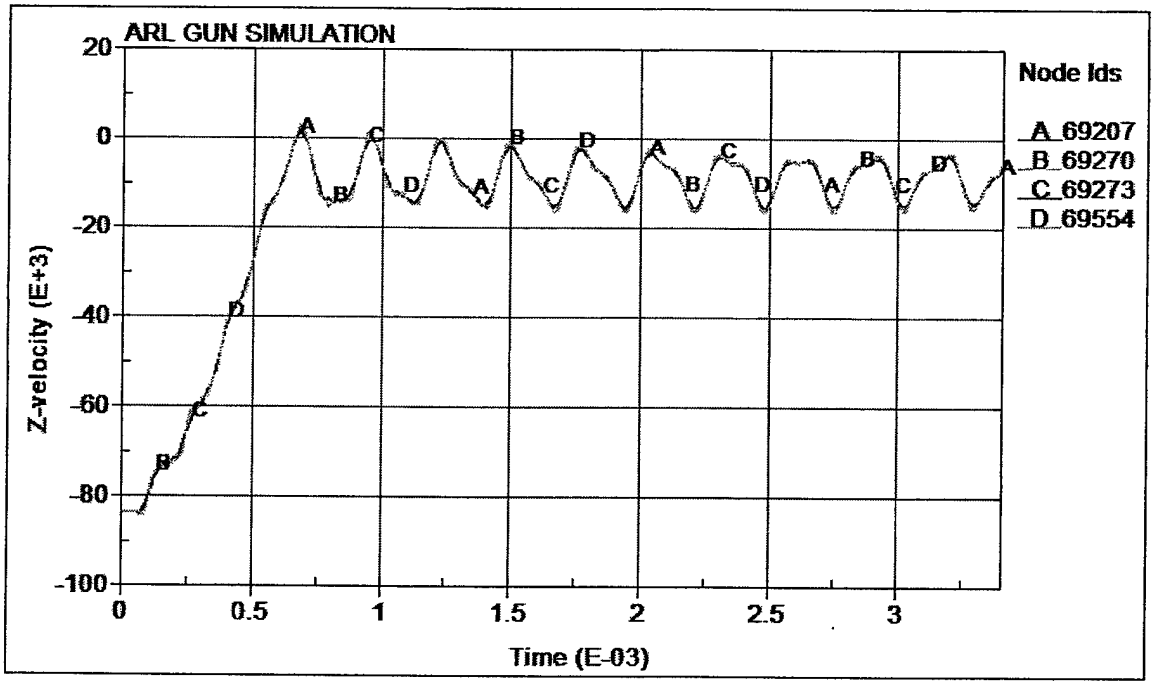

Figure 38. Velocity of the OBR as a function of time.

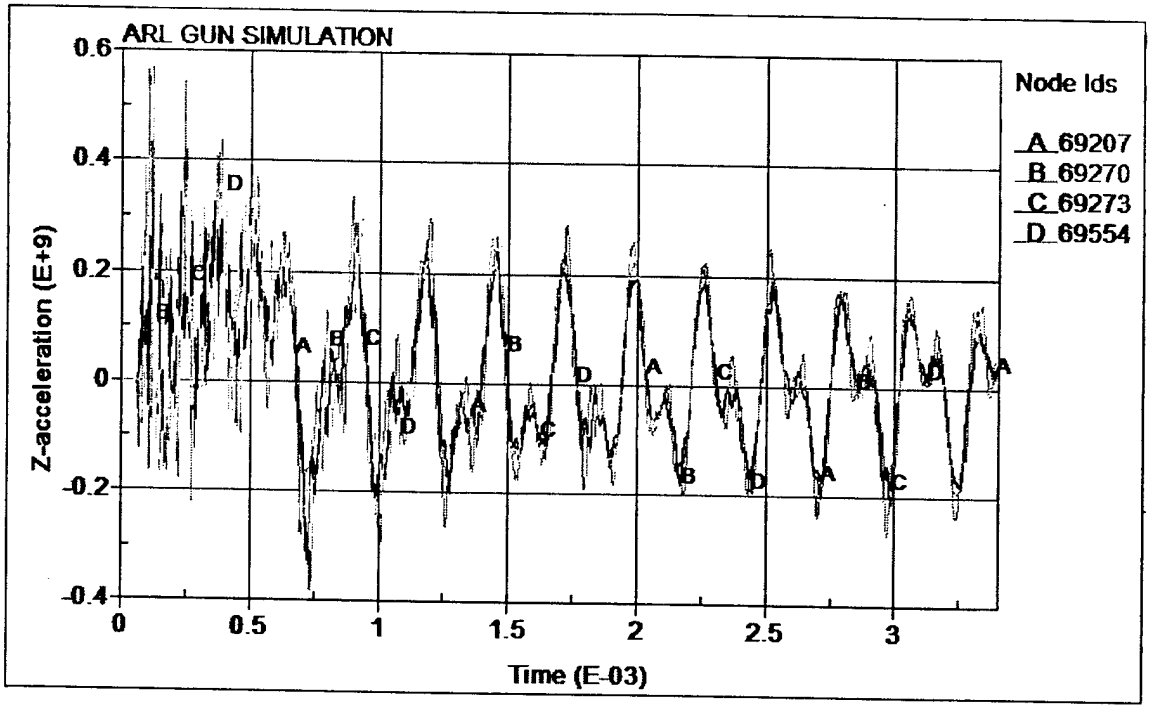

Figure 39. Acceleration of several nodes on the OBR.

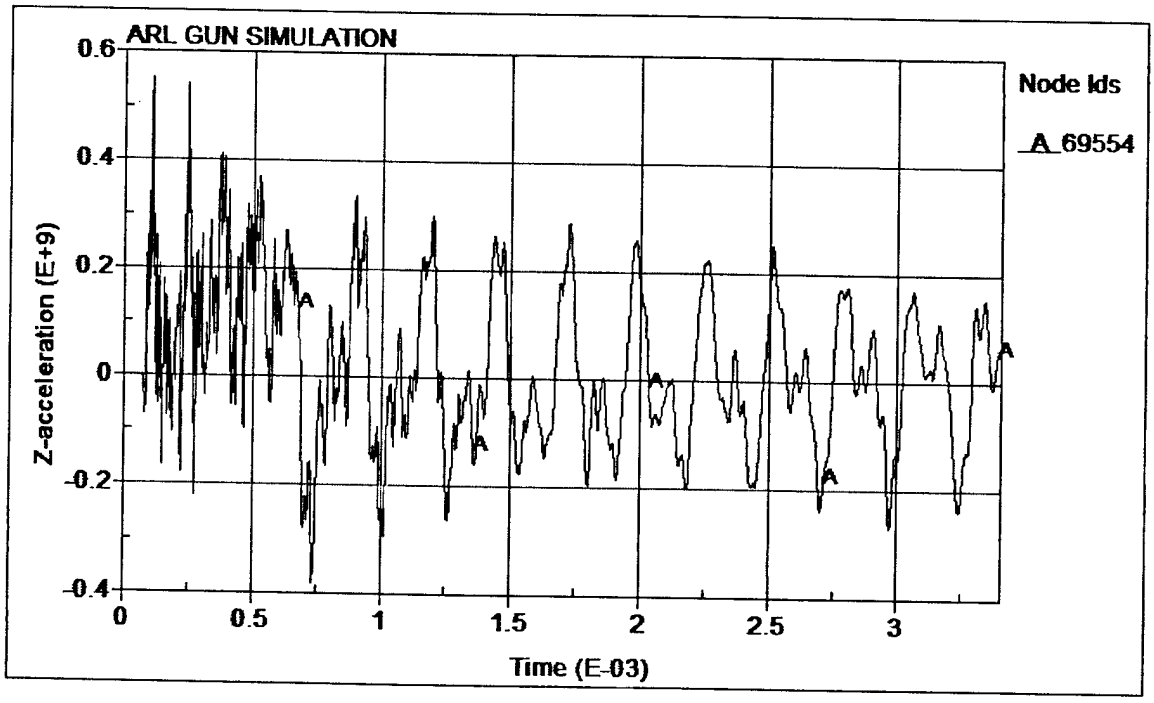

Figure 40. Acceleration of the top of the OBR.

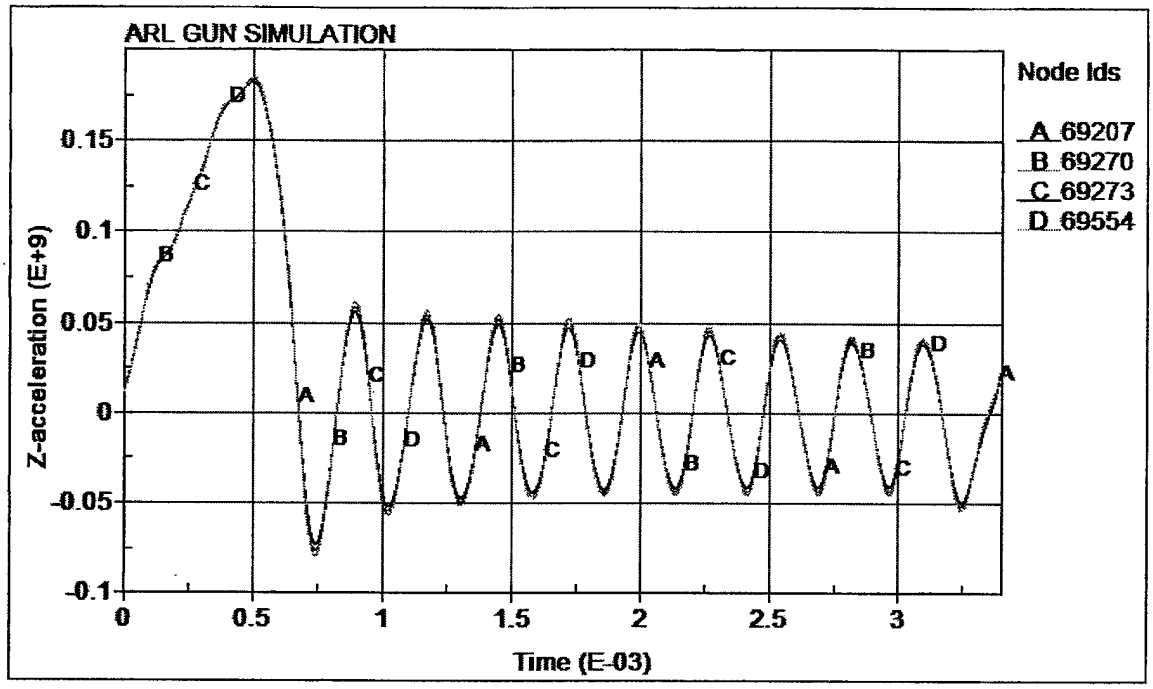

Figure 41. Acceleration of the top of the OBR filtered at 2500 Hz.

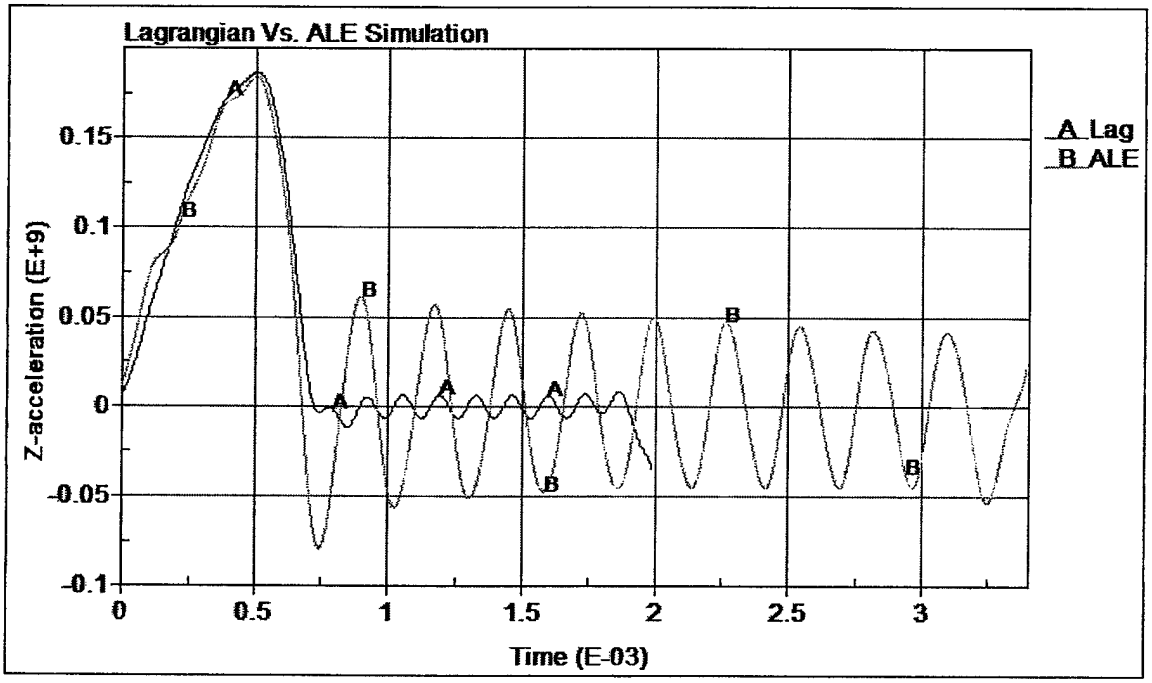

Figure 42. Acceleration of the top of the OBR filtered at 2500 Hz for both the Lagrangian and ALE simulations.

7. Model Validation: Simulation vs. Experiment

Several experimental tests were conducted at the ARL air gun facility located at Adelphi, MD. The air gun simulation is achieved using impact mitigation techniques whereby the component is propelled to a target inside a carrier equipped to measure component response during the simulation. The initial experimental setup was previously shown in Figure 2. The mitigator is placed in the catch tube and in contact with the MEM. The OBR is launched to impact the mitigator. Upon crush of the mitigator, it will push and repel the MEM in the opposite direction. The postexperiment view was shown in Figure 3. Acceleration data were collected on the top and the bottom of the OBR. The acceleration data obtained from the experiment on the top of the OBR are reported in Figure 43. This acceleration is filtered with low-pass filter with a cutoff frequency of 2500 Hz and shown in Figure 44.

The simulation results are compared with experiments qualitatively and quantitatively. Qualitatively, the deformation of the mitigator looks the same in the simulation and experiment. The experimental final crushed length of the mitigator is reported as 210.0 mm (8.27 in). The simulated final crushed length of the mitigator is predicted to be 226.0 mm (8.90 in), a difference of ~7% off from the actual crushed length.

The quantitative validation consists of comparing the acceleration data from simulation and experiment. The acceleration of the top of the OBR from simulation and experiment is shown in Figure 45. To find out the dominant frequencies in the response of the system the acceleration obtained from the simulation is treated with Fast Fourier Transform (FFT). The FFT is performed in LSPOST on the acceleration data and shown in Figure 46. One can observe that the second dominant frequency for the test spectrum is ~7000 Hz.

For comparison purposes, both the simulation results and the experimental results are filtered with low-pass cutoff frequencies of 7000 and 2500 Hz, respectively. The simulations and the experiment's acceleration of the top of the OBR for both filtrations are shown in Figures 47 and 48. Figure 47 shows a relatively good agreement between the predicted and test acceleration responses using material model 126 when a stress scaled factor of 1.5 was used in the analysis. A higher stress scale factor (1.5 instead of 1.2) has significantly attenuated the free vibration as indicated in Figure 47. Good prediction is observed from the simulation as compared to experiment, particularly for the 2500 cutoff frequency. Figure 48 compares several runs for the simulation. Two predictions are presented with material 126. The stress is scaled by 1.2 and 1.5 in the two predictions. One can observe that when the stress is scaled by 1.2, the peak acceleration is underpredicted. When the stress is scaled by 1.5, the peak acceleration is overpredicted. Figure 48 also shows the prediction of acceleration using material 63, with the stress scaled by 1.5 and the same overpredictive trend observed.

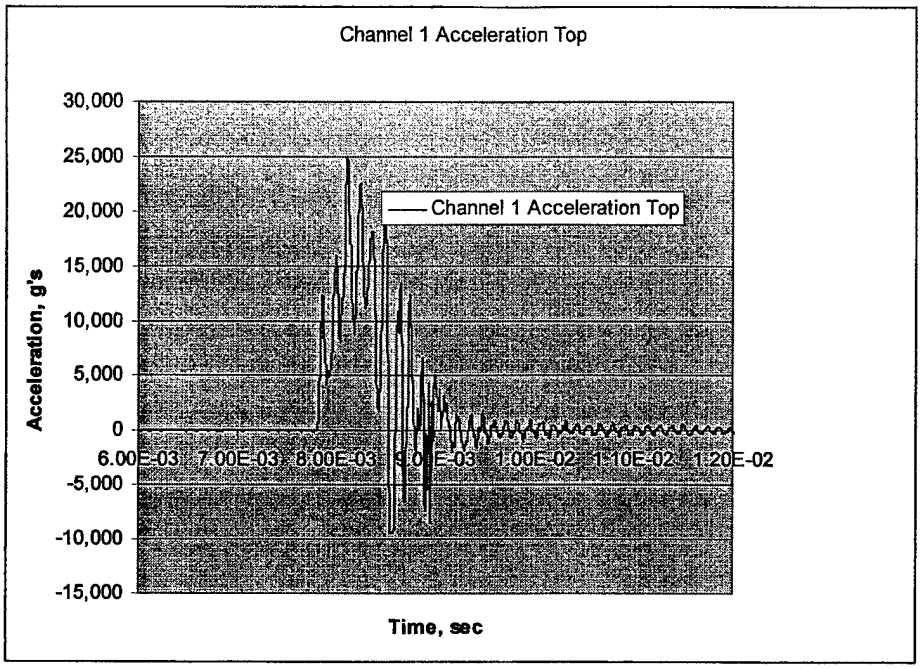

Figure 43. Top acceleration of the OBR.

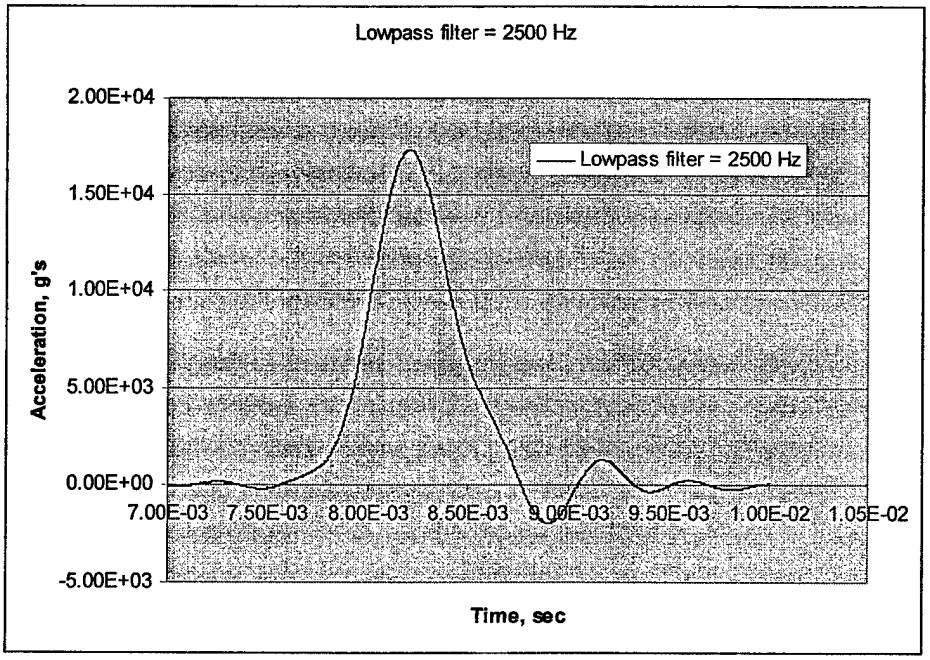

Figure 44. Top acceleration of the OBR filtered at 2500 Hz.

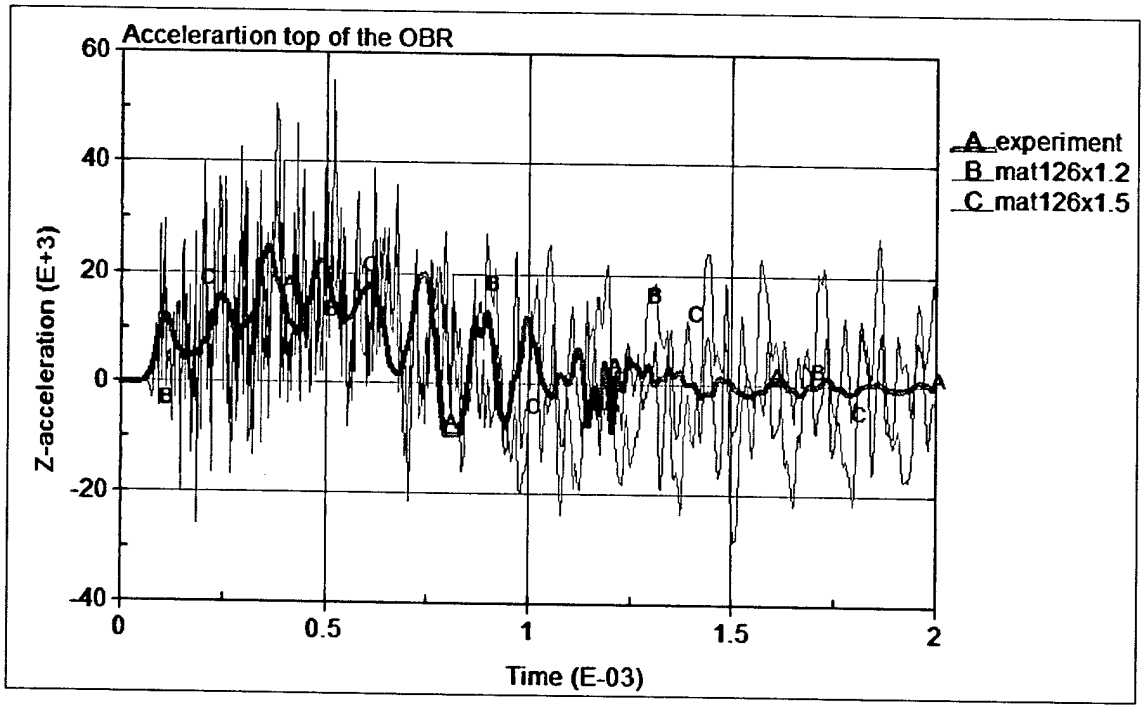

Figure 45. Acceleration of the top of the OBR, simulation vs. experiment.

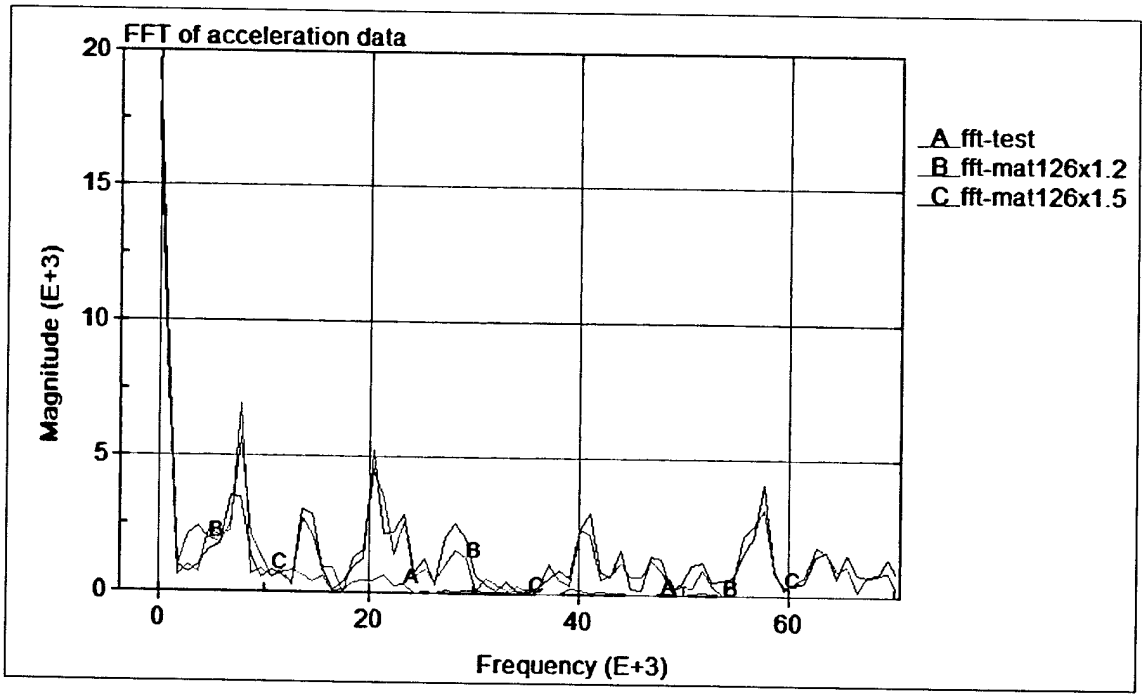

Figure 46. FFT of the experiment and simulation results.

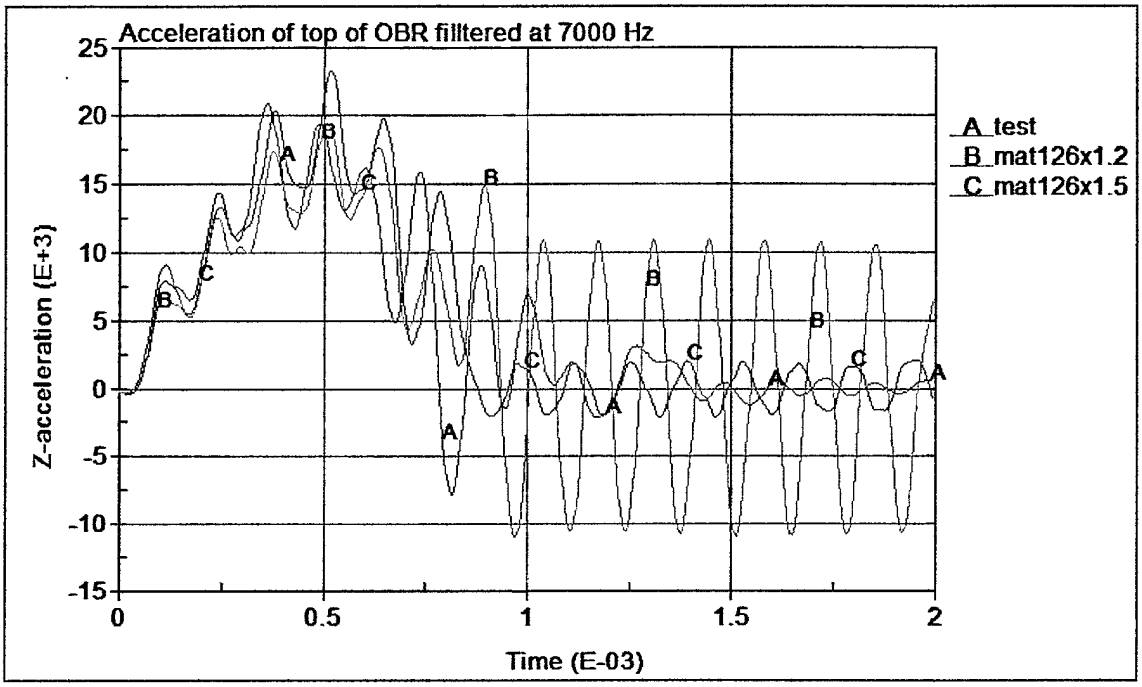

Figure 47. Simulation vs. experiment, acceleration of top of OBR filtered at 7000 Hz.

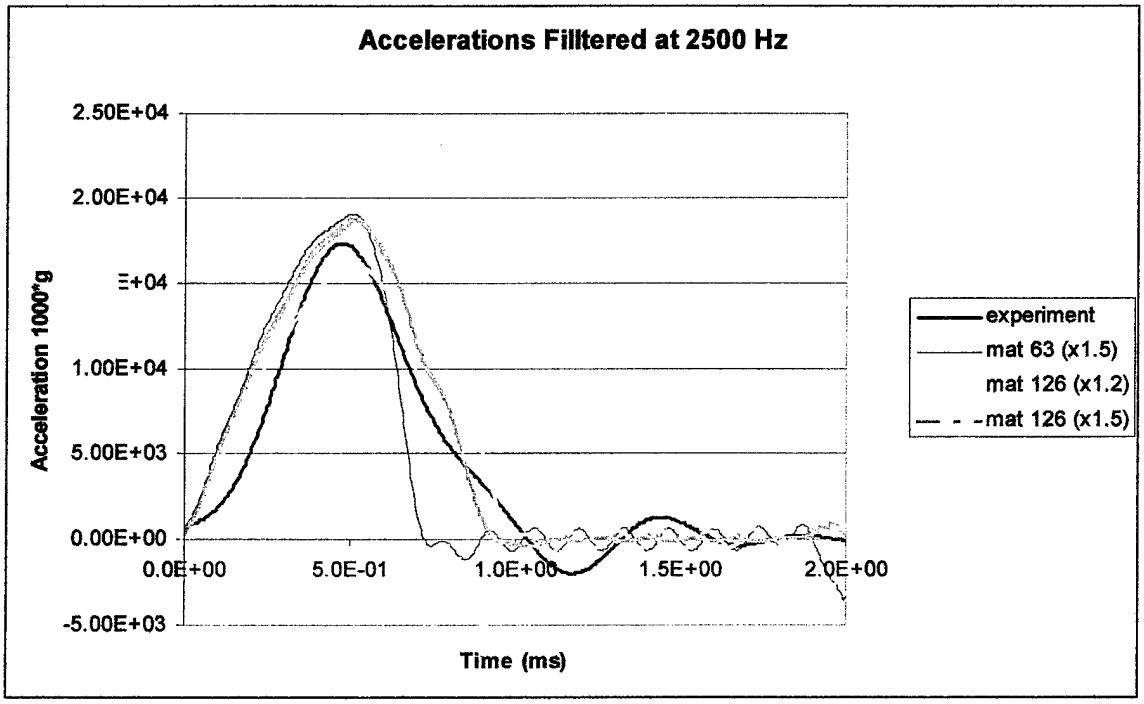

Figure 48. Simulation vs. experiment, acceleration of top of OBR filtered at 2500 Hz.

8. Physical Interpretations Using the FE Results

FE simulation results help explain the physics of the air gun launch simulation as described here. Figure 49 compares the displacement profiles for nodes corresponding to different parts on the air gun model. Deflection profile for nodes 118794 and 118259 on the test projectile shows a reversal in its motion direction from its highest peak at ~0.5 ms. Projectile motion for nodes 118794 and 118259 closely followed each other as indicated by the overlapping of their histories on the top of each other. Mitigator top edge node (77897) followed the deflection profile for the projectile nodes (118794 or 118259) until ~1 ms. This indicates that the top edge compressed as the projectile penetrated the crushing mitigator. At this instant, the energy from the system has been transmitted to the MEM, as it gained momentum, and the projectile bounced back. As seen in the plots for nodes 77897 and 118259, at ~1.1 ms, the mitigator crushed nodes at its tip (node 77897) did not bounce back as much as did the projectile itself. In essence, the mitigator remained in its original position at the end of the gun launch simulation. This phenomenon confirms the posttest observation as documented in section 3 (Figure 3). As indicated in the figure, the rates and magnitudes of deflections for mitigator nodes (77897, 1708, and 74544) starting from its tip of the wedge to the bottom end where the MEM is connected are different. The bottom part of the mitigator (node 74544) does not appear to have sensed the motion at least until ~0.4 ms after the initiation of the impact. The bottom of the mitigator (node 74544) moves together with the MEM (node 116926) until 0.9 ms, and then the mitigator starts moving back to its initial position. The MEM at this instant gains its momentum and shoots forward until being stopped at the rear retrieving end (Figure 3).

9. Conclusions

The objective of this effort was to develop an overall analytical model to predict the 3-D transient response of a generic artillery component subjected to launch simulation in the ARL air gun facility located at Adelphi, MD. The simulation was achieved using impact mitigation techniques whereby the component is propelled to a target inside a carrier equipped to measure component response during the simulation. Several LS-DYNA models were developed to simulate the air gun launch environment in which a test object mounted on a projectile is fired through the air gun and decelerated by crushing Al honeycomb mitigator which impacts the MEM before being stopped at the retrieving end. Two computational methods are employed for this purpose: the Lagrangian and ALE methods. The Lagrangian method is simpler to set up, postprocess, and requires less computational time. However, it requires significant expertise in the LS-DYNA code to make the simulation numerically stable. This is due to the significantly large deformation of the mitigator. On the other hand, the ALE method is more difficult to set

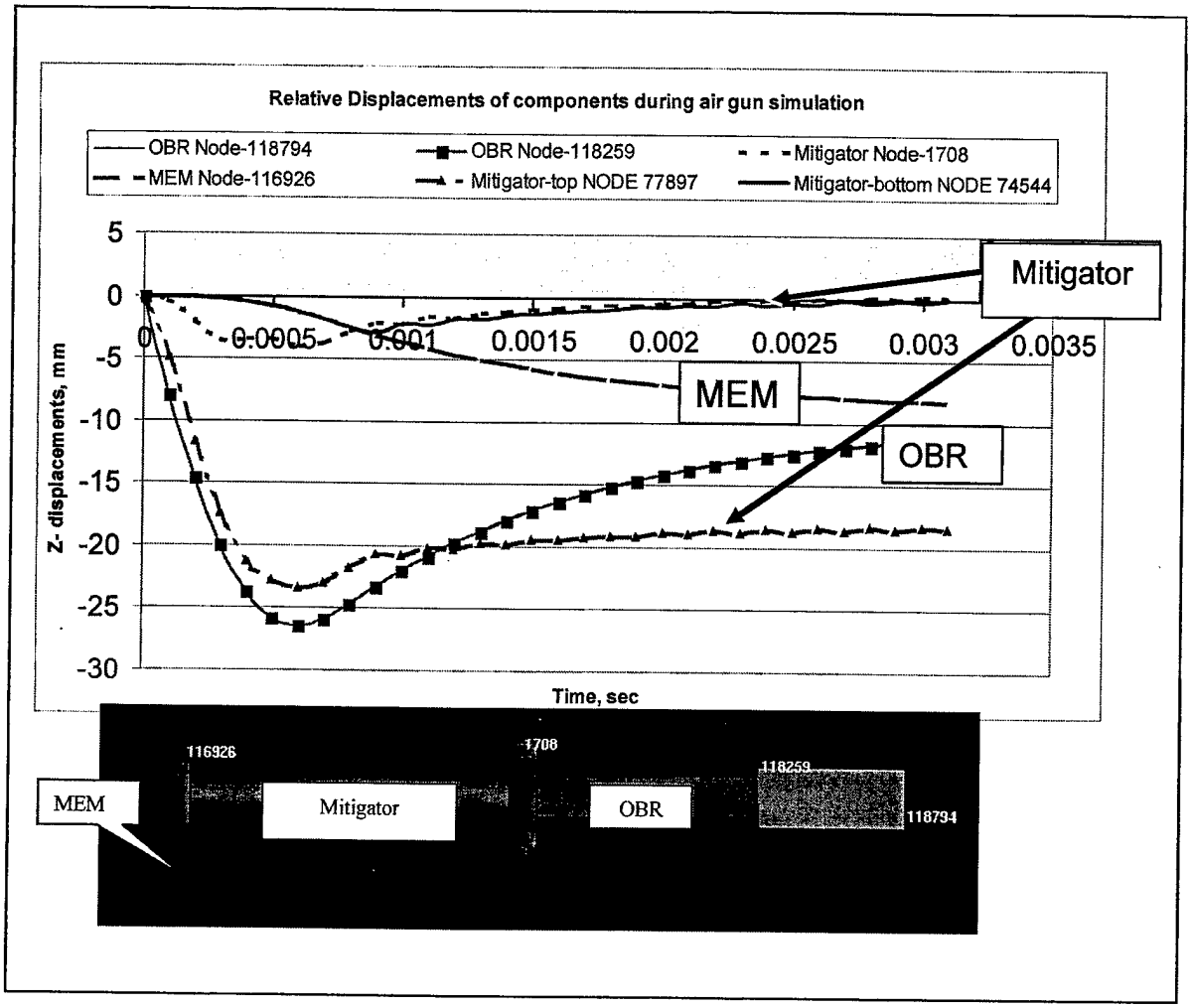

Figure 49. Plots of relative displacements for different parts of the air gun apparatus.

up, postprocess, and requires much more CPU time, but is more suitable for a very large deformation-like flow problem. Both computational methods led to the same prediction for the acceleration of the OBR.

Both material models 126 and 63 led to reasonable predictions and are able to simulate the behavior of the mitigator. The strain rate sensitivity must be accounted for in these simulations. If no strain rate effect is included, the peak acceleration of the OBR is underpredicted. In the presented simulation, instead of activating the rate effect in the material models, the stress is scaled by values between 1.2 and 1.5. This will have the same effect as if the rate effect is activated in the material model.

Good prediction of the oscillatory characteristics and peak acceleration of the OBR is achieved using the presented models and the methods employed. The LS-DYNA simulation code can be used for such problems with confidence that the code will aid in prediction of the proper response of any instrument mounted on the OBR.

10. Recommendations and Significance of the FE Model

Improvements on the LS-DYNA model presented in this report are needed to address its limitations and capture the high-frequency transient phenomena that are typical during launch-simulation air gun tests. Once the improvements are incorporated in the current air gun FE model, it will significantly enhance ARL's capability to address the customer's need in explaining projectile behavior during an air gun test and will be useful in facilitating design and preparation of an effective air gun test. The following are a few of the suggested improvements for the simulation methodology:

- Investigate damping effect on the response (mass and stiffness proportional damping) of the test article in an air gun simulation test,
- Characterize material performance for Al honeycomb mitigator from high-rate compression test results,
- Investigate high-frequency contribution on the response of the test article,
- Develop a roadmap for modeling different gun calibers, and
- Calibrate FEM with the measured strain data.

A complementary use of the virtual simulation code could be useful in facilitating design and preparation of an effective air gun test. A virtual model could aid in pre- and posttest investigation as well. Pretest investigation using an FE model is important in designing and selecting proper test configurations and physical operating parameters of an air gun test environment. These physical operating parameters include the projectile velocity, the physical characteristics of the MEM, and/or the physical characteristics of the mitigator. The ability to numerically simulate the dynamic response of the test item will allow the physical operating parameters of the air gun test environment to be tuned to achieve the specific dynamic conditions that are required for each particular test item. This will significantly reduce the number of test results that are deemed unusable due to a failure to meet the required dynamic conditions. In addition, it is anticipated that the posttest investigation using the numerical simulation model will help explain the source of certain undesirable high-frequency phenomena that are typically measured during air gun tests. Furthermore, the full-field results will aid the test designer in choosing the optimal locations for the limited number of transducers that can be applied to the test item, thereby ensuring that the most useful data are measured in each test.

11. References

1. Lu, W.-Y.; Hinnerichs, T.; Crush of High Density Al Honeycombs; Presented at the International Mechanical Engineering Congress and Exposition, New York, NY, 11–16 November 2001.

2. Hallquist, J. O. *LS-DYNA Theoretical Manual*; Livermore Software Technology Corp.: Livermore, CA, 1998.

3. Hallquist, J. O. *LS-DYNA User's Manual*; Livermore Software Technology Corp.: Livermore, CA, 1998; Vol. 1.

4. Hallquist, J. O. *LS-DYNA User's Manual*; Livermore Software Technology Corp.: Livermore, CA, 1998; Vol. 2.

5. Tabiei, A. Cincinnati, OH. Advanced LS-DYNA Lecture Notes; Livermore Software Technology Corp: Livermore, CA, 1999–2002.

6. Bitzer, T. *Honeycomb Technology*; Chapman and Hall: London, UK, 1997.